THE PENNSYLVANIA STATE UNIVERSITY
SCHREYER HONORS COLLEGE

DEPARTMENT OF BIOLOGY

Investigating a Mysterious Retention of Photosynthesis in the Parasitic Plant *Cuscuta gronovii*

LEO GOUBET-MCCALL
SPRING 2024

A thesis
submitted in partial fulfillment
of the requirements
for a baccalaureate degree
in Biology
with honors in Biology

Reviewed and approved* by the following:

Claude W. dePamphilis
Professor of Biology
Thesis Supervisor

James H. Marden
Professor of Biology
Honors Advisor

Tomás A. Carlo Joglar
Professor of Biology
Faculty Reader

*Electronic approvals are on file.

ABSTRACT

The stem parasitic plant *Cuscuta gronovii* is largely considered to be holoparasitic due to its characteristic yellow stems and total reliance on a host for survival. However, several tissues exhibit greening at various points in *C. gronovii*'s life cycle, similar to several other *Cuscuta* species. This greening, as well as the maintenance of key photosynthesis genes, suggests that *C. gronovii* has more photosynthetic capability than previously expected, and may be using its limited photosynthetic apparatus to drive nutrient accumulation in seeds. In particular, previous research has suggested that the RuBisCO shunt, an alternate pathway utilizing RuBisCO and the energy from photosynthesis to efficiently generate lipids for seed filling, may be active in *Cuscuta* species. This thesis seeks to evaluate this hypothesis using multiple lines of evidence. Putative orthologs for several pathways of interest—photosynthesis, chlorophyll and lipid synthesis, RuBisCO shunt, and Calvin cycle—were identified in *C. gronovii*, and their expression across fruit and seedling development was measured using transcriptome data. Stable isotope tracking experiments were used to confirm RuBisCO activity in floral and fruit tissues, and evidence for chlorophyll pigments was found in different green tissues. While the question of the RuBisCO shunt's activity is still unclear, these experiments provide clear evidence for photosynthetic activity in *C. gronovii* and open up many avenues for future research.

TABLE OF CONTENTS

LIST OF FIGURES

LIST OF TABLES

ACKNOWLEDGEMENTS

I would first like to thank my research advisor, Claude dePamphilis, for all that you have taught me over the past two and half years. Thank you for bringing me into the incredible world of plant biology, and for giving me the space and resources to explore. Thank you also to Tomás Carlo and Gabrielle Monshausen, for taking the time to teach me new techniques and help expand the scope of this project. You helped me bring my project into new and fascinating areas that I had never expected to explore, and in doing so greatly enriched my learning.

Thank you also to Paula Ralph, Juan Cerda, and Elizabeth Kelly for helping me with some of the numerous logistical, bioinformatics, and data analysis problems that popped up during my time in the lab. Thank you as well to the rest of the dePamphilis lab for the many interesting conversations during lab meetings, all of which have helped me commit to my path of becoming a scientist.

Last but not least, thank you to my family and friends for all your support and the many care packages, hikes, concerts, and climbing sessions over the past few years. Thank you especially to Sophia for helping me get through the past few semesters, and for supporting me through it all.

Chapter 1

Introduction and Literature Review

Heterotrophy in plants is a lesser-known adaptation that nevertheless can produce exceptionally varying patterns of growth and development. Many of the "rules" of plant growth have been circumvented by plant parasites, beginning with what could be considered the defining feature of green plants: photosynthesis.

1.1 Photosynthesis and Carbon Fixation in Plants

Photosynthesis is far and away the most prevalent form of autotrophy on the planet, forming the base of nearly every ecosystem. Photosynthesis in eukaryotes originated through endosymbiotic capture of ancient cyanobacteria, in which an ancestral eukaryote engulfed a cyanobacterium (currently believed to be a relative of genus *Gloeomargarita*) without killing it (Sánchez-Baracaldo et al., 2017). Molecular clock studies show that the transition from this initial endosymbiotic event and the first true photosynthetic eukaryote would have taken about 200 million years, during which the chloroplast and host became completely dependent on one another (Sánchez-Baracaldo et al., 2017). This eventually produced many photosynthetic lineages including red and brown algae, dinoflagellates, diatoms, and green algae—the sister lineage to land plants (Blankenship, 2010; McFadden, 2001). Over the course of their evolution, chloroplasts became completely reliant on their hosts for survival, as most of the ancestral cyanobacterial genes were functionally transferred to the host's genome (Wicke et al., 2011). As

such, modern plastid genomes only encode around 100 distinct genes—which are fairly well-conserved and are often used to construct plant phylogenies—and the vast majority of the proteins required for plastid function are transcribed and translated from original endosymbiont genes that are now nuclear-encoded (Wicke et al., 2011).

The mechanisms of photosynthesis vary among the various photo-autotrophic lineages (which include several different bacterial lineages in addition to cyanobacteria) but are well conserved among green algae and plants (Blankenship, 2010). This begins with the absorption of photons using a network of pigments (various chlorophylls) and the transfer of this energy to a reaction center, photosystem II (M. P. Johnson, 2016). This reaction center splits water molecules into O_2 and H^+ ions and shuttles electrons to subsequent reaction centers, forming an electron transport chain analogous to that used in cellular respiration (Fig. 1A) (M. P. Johnson, 2016). This electron transport chain is ultimately used to produce ATP (using a H^+ gradient across the thylakoid membrane) and NADPH molecules, both of which are used in subsequent Calvin cycle reactions (M. P. Johnson, 2016).

The most important form of carbon fixation in land plants takes place during the Calvin (Calvin-Benson-Bassham, CBB) cycle, making use of the ubiquitous enzyme ribulose-1,5-bisphosphate carboxylase/oxygenase (RuBisCO) (Fig. 1B). In this cycle, the NADPH and ATP produced during the light reactions are used to drive the conversion of CO_2 into glyceraldehyde 3-phosphate (G3P), which is eventually converted into sucrose to be used by the rest of the plant; the essential carbon fixation step, in which CO_2 is incorporated into an intermediate molecule, is performed by RuBisCO, making this a protein of particular interest for crop studies (Parry et al., 2013).

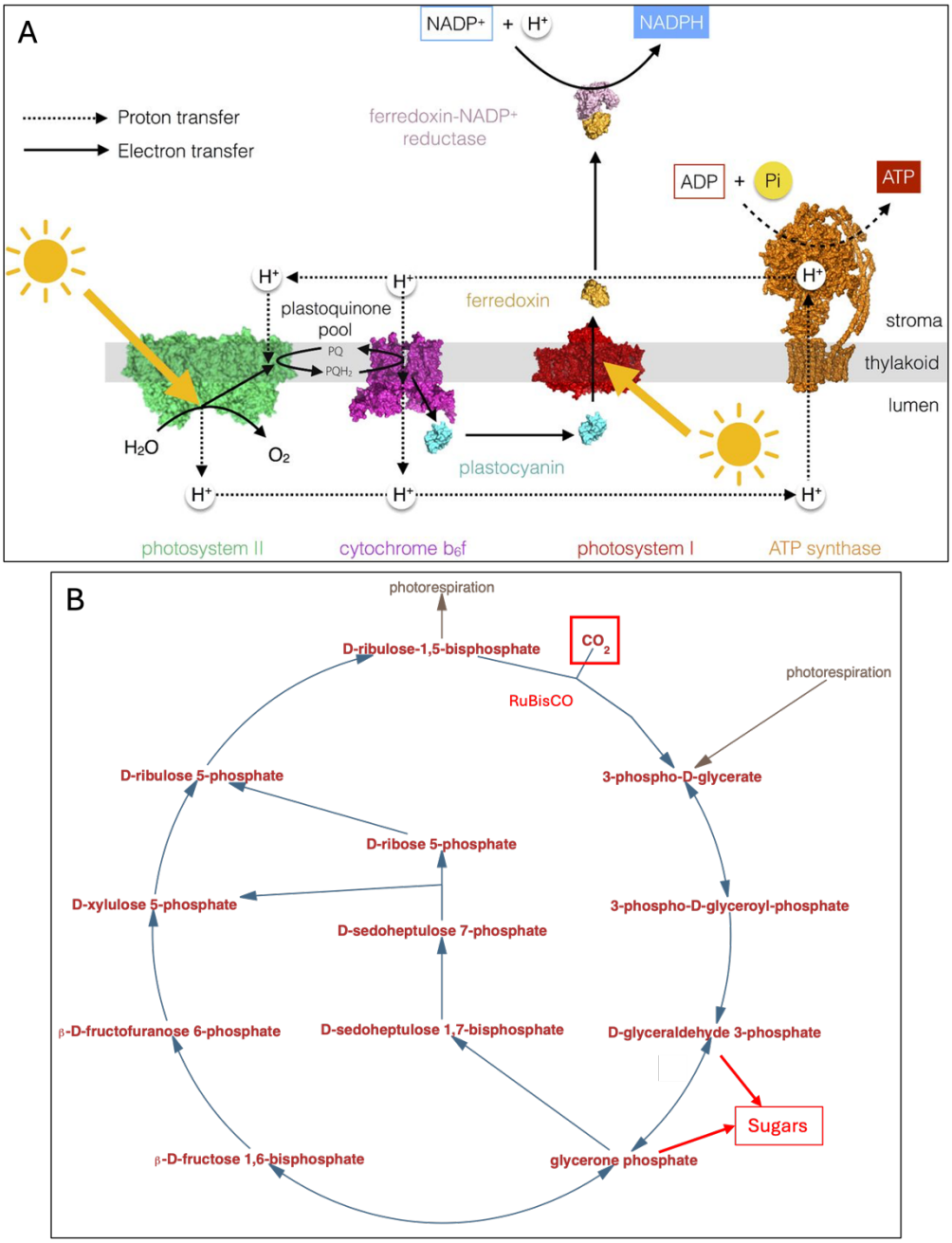

Figure 1. Overview of the reactions of photosynthesis. A: reaction centers and electron transport chain of the light-dependent reactions, from M. P. Johnson (2016). B: main reactions and products of the Calvin cycle, modified from PlantCyc database (Plant Metabolics Network (PMN), n.d.).

Despite its importance, RuBisCO is fairly inefficient due to its residual oxygenase activity, which produces wasteful by-products that a plant must manage through photorespiration (Parry et al., 2013). This inefficiency has led to the evolution of workarounds such as C_4 and CAM photosynthesis by many lineages of plants (Parry et al., 2013). Both of these methods involve variations in leaf morphology and function in order to separate the initial fixation of CO_2 from RuBisCO activity. Both plants use phosphoenolpyruvate (PEP) carboxylase to initially fix CO_2 from the atmosphere into a 4-carbon compound—oxaloacetate and eventually malate—which is either stored or transported for later use (Ludwig et al., 2024). CAM plants, being mostly adapted to highly arid conditions (such as most cacti), perform this carbon fixation and all necessary gas exchange at night, when water loss through stomata is less significant; in the day, when light energy is abundant, stored malate is converted back into CO_2 for use by RuBisCO in the Calvin cycle (Ludwig et al., 2024). Standard C_4 plants (such as Poaceae in the monocots and Amaranthaceae in the dicots) separate these processes spatially by transporting malate into a specialized cell (bundle-sheath cells) that contains RuBisCO and the rest of the Calvin cycle machinery; in this way, CO_2 is concentrated spatially around RuBisCO to limit its access to O_2 and reduce inefficiency due to photorespiration (Ludwig et al., 2024).

This alternate CO_2 metabolism, in both CAM and C_4 plants, leads to significant differences in the ratio of carbon isotopes that are incorporated by the plant. C_4 plants in particular (as well as CAM plants, to a lesser extent) typically contain a much higher concentration of ^{13}C than C_3 plants—this is because RuBisCO selectively avoids using ^{13}C-containing CO_2, whereas PEP carboxylase is much less selective (O'Leary, 1981). Concentrating ^{13}C-containing CO_2 around RuBisCO results in sugars (and eventually entire plant tissues) that

contain a higher percentage of ^{13}C (referred to as $\delta^{13}C$) than would otherwise be found in C_3 plants (O'Leary, 1981). This photosynthesis-dependent isotope fractionation is widely used in ecology to track carbon and energy usage across ecosystems and can be easily incorporated into plant biology experiments by applying ^{13}C-enriched compounds, such as urea (Kelleway et al., 2018; Schmidt & Scrimgeour, 2001).

1.2 Parasitism in Angiosperms

Parasitism in angiosperms develops through two main modes, haustorial parasitism and mycoheterotrophy. Each of these adaptations has evolved numerous times in many different lineages ranging across the plant tree of life (Barkman et al., 2007; Merckx & Freudenstein, 2010; Nickrent, 2020). Mycoheterotrophy, in which a plant takes advantage of an existing mycelial network to steal nutrients and organic compounds from neighboring plants and fungi, is most common in monocots, though some mycoheterotrophs are eudicots as well (e.g., *Monotropa* spp. found in the East Coast of the Unites States) (Jąkalski et al., 2021). These plants, most of them within Orchidaceae, are often characterized by loss of photosynthesis and chlorophyll, and can exhibit very colorful and unusual shapes as a result; without the constraint of photosynthesis, there is no longer a need to develop and display functional leaves (Merckx et al., 2009).

Haustorial parasitism, which likewise is widespread across several lineages in the eudicots, produces arguably even more varied shapes and structures depending on the degree of parasitism (Barkman et al., 2007). The haustorium is a specialized root-like organ produced by all parasitic plants which is used to grow into a host and attach to its vasculature, providing an

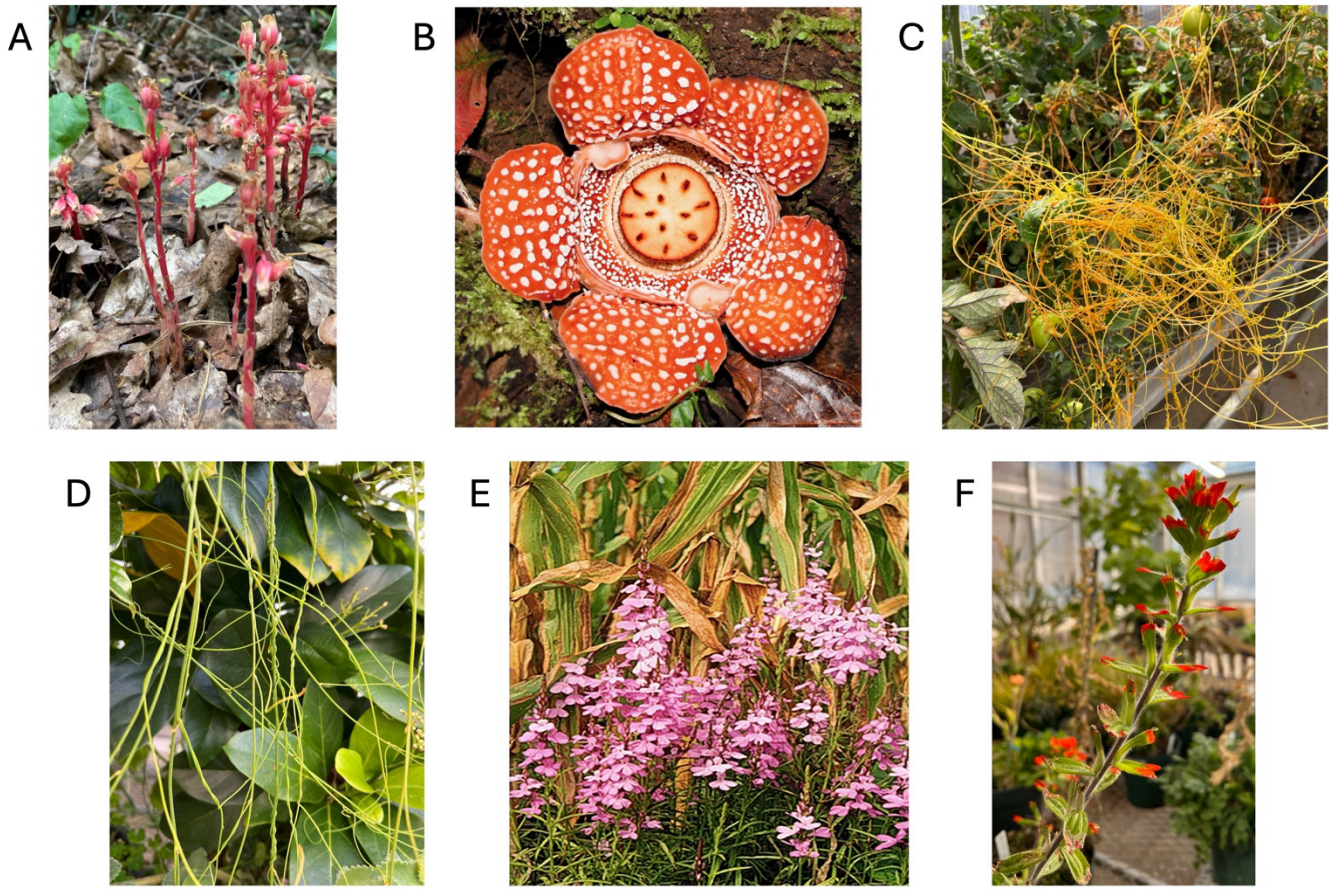

Figure 2. Morphological diversity of various parasitic and mycoheterotrophic plants. Pinesap, *Hypopitys monotropa,* a mycoheterotroph (A). *Rafflesia lagascae*, an endoparasite (from Molina et al., 2014) (B). Stem haustorial parasites *Cuscuta gronovii* (C) and *Cassytha filiformis* (D). Root haustorial parasites *Striga hermonthica* (from Makaza et al., 2023) (E) and *Castilleja coccinea* (F), both in family Orobanchaceae.

easy route through which photosynthate, water, and other nutrients can be stolen (Furuta et al., 2021). The most extreme and host-dependent (obligate) parasites are endoparasites (e.g., *Rafflesiaceae*, *Pilostyles*), which live entirely within a host plant's tissues until the production of reproductive structures (Teixeira-Costa et al., 2021). Another recurring form of parasitism is the production of vine-like tendrils to wrap around a host and form many haustorial connections—the two notable genera using this strategy, *Cuscuta* and *Cassytha* also exhibit highly reduced or nonexistent roots (Kuijt, 1969; Yuncker, 1932; Zhang et al., 2022). Haustorial parasitism can also

be divided into shoot- and root-parasitism, depending on the host structure that is invaded by haustoria. The most notable root parasites include the Orobanchaceae family, which includes several extremely damaging parasites such as *Striga* and *Orobanche*—a significant body of work is dedicated to protecting crop plants from these parasites (Goyet et al., 2019).

Haustorial parasites can be roughly divided into hemi- and holo-parasites, depending on the degree of parasitism exhibited by the plant. This is generally evaluated on the basis of photosynthetic ability and chlorophyll production, rather than on parasite independence. For example, *Cassytha* species are considered obligate parasites due to a lack of functional roots and their inability to survive and reproduce without a host, but hemi-parasitic because they exhibit some photosynthetic activity to supplement the nutrition received from a host (Zhang et al., 2022). This hemi-to-holo range is characterized by clear stages in plastid genome evolution, known as the "parasitic reduction syndrome" (Wicke & Naumann, 2018). These patterns, which are shared by haustorial parasites and mycoheterotrophs, include a gradual reduction in plastome size, and relatively predictable gene loss and pseudogenization as parasites become obligate and more fully heterotrophic: NADPH dehydrogenase (*ndh*) genes are typically lost first, followed by RNA polymerase (*rpo*) and core photosynthesis genes (e.g., *pet*, *psa*, and *psb* genes), ATP synthase genes, and genes involved in plastid translation (e.g., *trn*, *rpl*, *rps*, and *rrn*) (Wicke et al., 2011; Wicke & Naumann, 2018). Unsurprisingly, the most drastic plastid genome reductions can be found in endoparasites, which exhibit the most extreme form of heterotrophy: a recent *Pilostyles boyacensis* plastome sequence is only 12,047 bp in size (compared with *Arabidopsis thaliana* col, at 154,478 bp), and several *Rafflesiaceae* species are thought to have entirely lost

their chloroplast genomes (Arias-Agudelo et al., 2019; Guo et al., 2023; Molina et al., 2014; Sato et al., 1999).

1.3 The Genus Cuscuta

The genus *Cuscuta* (dodders) contains around 200 species spread throughout the world, and as such is one of the largest genera of parasitic plants (Yuncker, 1932). The genus is distinguished by yellow, tendril-like stems which wrap around a host before forming haustorial connections. *Cuscuta* uses these connections, similarly to other parasitic plants, to steal photosynthate and water, as well as to exchange a wide variety of organic molecules (such as micro-RNAs) that are involved in suppressing host defense responses (N. R. Johnson & Axtell, 2019; Shahid et al., 2018). All *Cuscuta* are obligate parasites, and many species are considered to be holoparasitic (McNeal et al., 2007a; Vogel et al., 2018).

Cuscuta falls completely within the Convolvulaceae family, which includes many well-known and agriculturally important plants such as sweet potato (*Ipomoea batatas*) and morning-glories (several species within various genera including *Ipomoea* and *Convolvulus*) (Simões et al., 2022). The phylogeny of *Cuscuta* has been notoriously difficult to resolve precisely due to various polyphyletic groups and very subtle morphological variation, but the genus can be clearly sorted into four subgenera; *Monogyna*, *Cuscuta*, *Grammica*, and *Pachystigma* (Costea et al., 2015; McNeal et al., 2007a; Stefanović et al., 2007). The largest of these, subgenus *Grammica*, contains several species of note including *C. campestris*, *C. pentagona*, and *C. gronovii*—the subject of this thesis. *C. campestris* (field dodder) and *C. pentagona* (five-angled dodder) are both notorious agricultural parasites and are capable of drastically reducing yields

for crops while being difficult to eradicate (Costea & Tardif, 2006; Fernández-Aparicio et al., 2020; Lanini & Kogan, 2005).

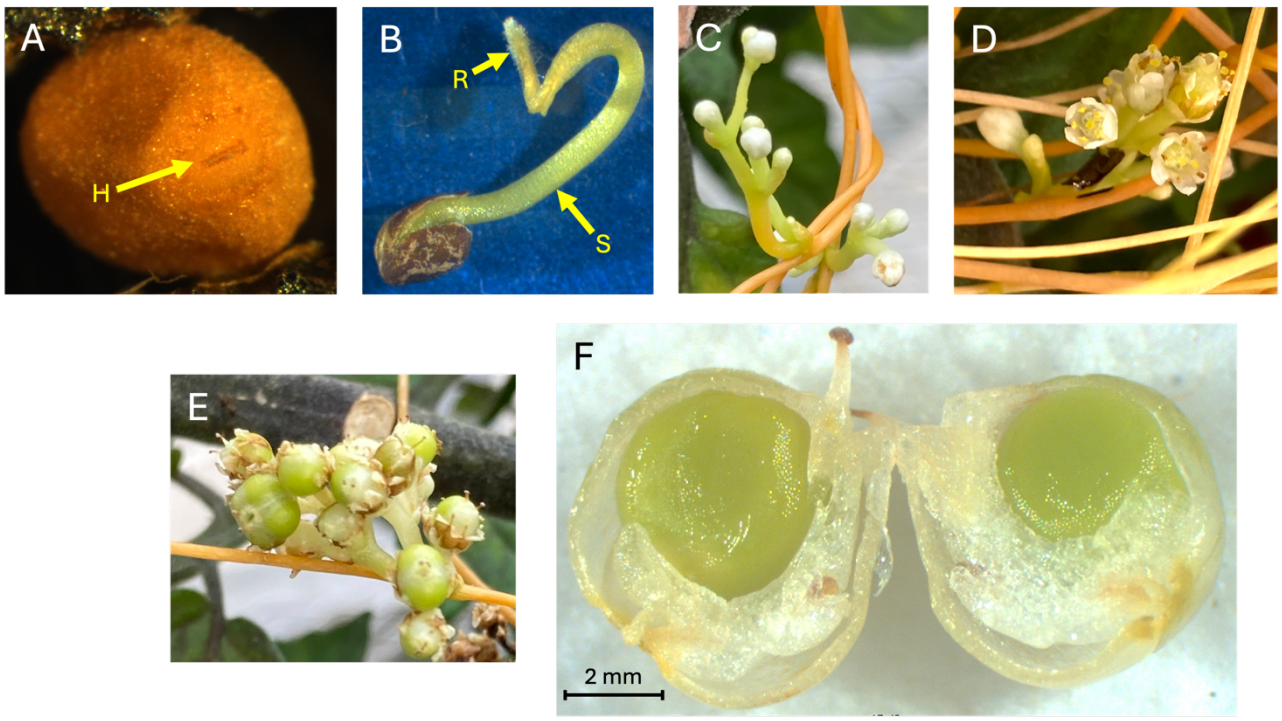

Figure 3. Notable green tissues in *C. gronovii*. Tissues are shown in order of development: dry seed (A), early seedling (B), early flowers with green peduncles (C), open flower/early fruits (D), and maturing green fruits (E). A dissection of a mature fruit (F) showing the outer "fruit cover" layer and the bright green seeds. Features: H, seed hilum; R, seedling radicle; S, seedling shoot.

C. gronovii (swamp dodder) has a much smaller range—mainly in North America along with some regions in Europe—and can be a parasite of some crops such as cranberries and blueberries across the East Coast of the United States (Costea & Tardif, 2006; Sandler, 2010). Outside of agriculture, however, *C. gronovii* is more notable as a native plant that can potentially play an important role in maintaining the diversity of surrounding ecosystems; several other dodder species have been described as "ecosystem engineers" due to the way they reduce the prevalence of dominant plants, thus increasing overall diversity (Costea et al., 2023; Press & Phoenix, 2005). This is complicated by the fact that *C. gronovii* is a polyphyletic group

containing several potential subspecies, some of which may be more aggressive parasites than others (Costea et al., 2023).

The mystery of *C. gronovii*'s lifestyle deepens when considering its anatomy and development. All *Cuscuta* species are obligate parasites and many—including *C. gronovii* and most of its relatives in subgenus *Grammica*—are considered holoparasitic. Despite this, *C. gronovii* shows clear greening in several different tissues (Fig. 3), most notably in the developing fruit, suggesting chlorophyll synthesis and some residual photosynthetic activity. Along with this, several *Cuscuta* species have maintained many important plastid-encoded photosynthesis genes including most if not all photosystem genes, and the large subunit of RuBisCO (McNeal et al., 2007a,b). Similarly interesting patterns of gene loss and retention are found in the nuclear genome of *C. campestris*. Vogel et al. (2018) showed that *C. campestris* has lost many genes with a large variety of functions including photosynthesis, lipid metabolism and transport, and RNA regulation, including many genes important for high-light-intensity photosynthesis. However, *C. campestris* has also retained the genes for several complete photosynthesis light reaction pathways, as well as chlorophyll and carotenoid synthesis pathways, clearly showing that maintenance of photosynthesis goes beyond a few genes in the chloroplast genome (Vogel et al., 2018).

The long-term maintenance of a photosynthetic apparatus in most *Cuscuta* species must have some purpose, and McNeal et al. (2007a,b) hypothesized that this can be linked to lipid synthesis for seed filling. Seed development and filling in *Cuscuta* often occurs when the host plant is declining and unable to provide all the necessary photosynthate—flowering in many *Cuscuta* species is known to be dependent on or otherwise related to host flowering patterns,

which often results in *Cuscuta* species flowering at or near the end of the host's reproductive cycle (Costea & Tardif, 2006; Shen et al., 2009). Thus, a secondary pathway for lipid synthesis would be highly beneficial to produce a higher number of viable seeds. This hypothesis was based on a then-novel pathway to produce lipids using RuBisCO and the light reactions of photosynthesis, known as the RuBisCO shunt (Schwender et al., 2004).

1.4 The RuBisCO Shunt

The RuBisCO shunt is a metabolic pathway that was first described in *Brassica napus* by Jörg Schwender and colleagues in 2004, using a series of carbon labeling and tracking experiments. Similarly to glycolysis, this pathway ultimately converts glucose-6-phosphate (or fructose-6-phosphate) into pyruvate—this pyruvate is then used to produce acetyl-CoA, which is used as a precursor for various lipid molecules including fatty acids (FA) and triacylglycerols (TAG), which make up one of the most important storage lipids in seeds (Baud, 2018). In typical glycolysis-mediated pyruvate synthesis, a significant portion of the carbon used in the pathway is lost as CO_2 when pyruvate is converted to acetyl-CoA by the pyruvate dehydrogenase complex; one CO_2 molecule is produced and lost for every acetyl-CoA synthesized (Baud, 2018; Schwender et al., 2004). However, the RuBisCO shunt pathway allows plants to recapture this CO_2 and recycle it to produce more pyruvate, along with recycling CO_2 produced through cellular respiration—the RuBisCO shunt is estimated to provide 20% more acetyl-CoA for a 40% reduction in CO_2 loss. (Schwender et al., 2004). This pathway thus allows plants to produce seed lipids more efficiently utilizing enzymes that have been cannibalized from other pathways,

including glycolysis, the pentose phosphate pathway, and the Calvin cycle (Fig. 4) (Plant Metabolic Network (PMN), n.d.).

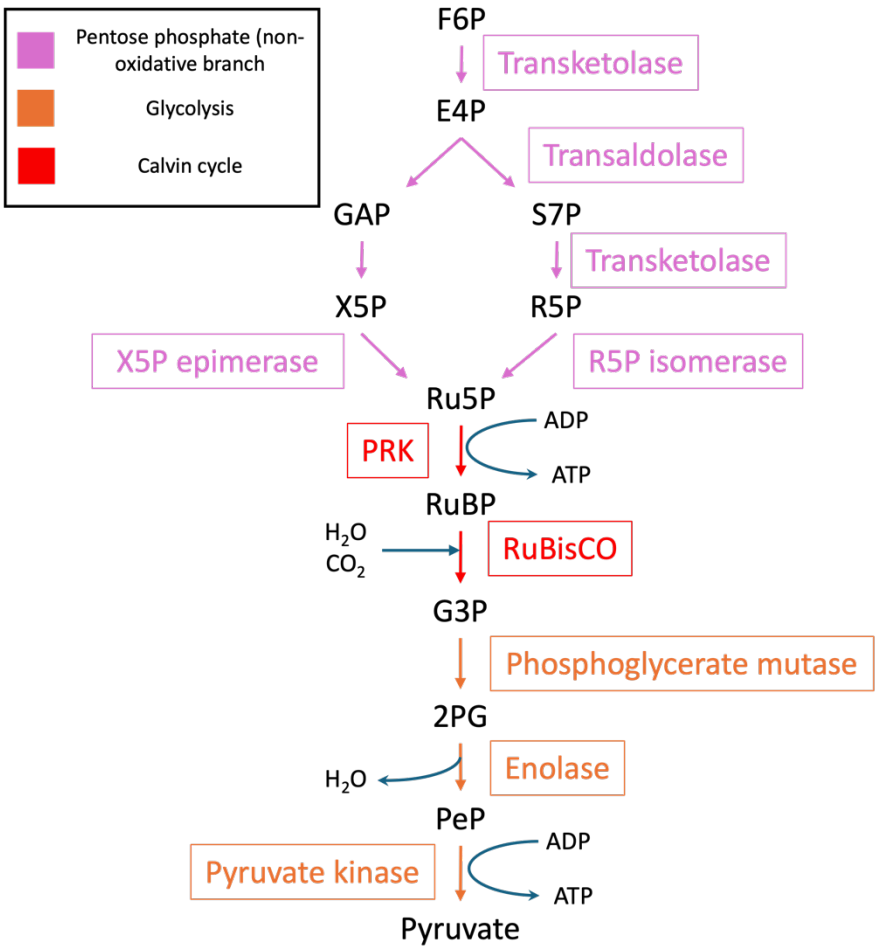

Figure 4. Overview of the RuBisCO shunt, showing the origins of each gene involved in the pathway. Molecules involved: F6P, fructose 6-phosphate; E4P, erythrose 4-phosphate; GAP, glyceraldehyde 3-phosphate; S7P, sedoheptulose 7-phosphate; R5P, ribose 5-phosphate; Ru5P, ribulose 5-phosphate; RuBP, ribulose-1,5-bisphosphate; G3P, 3-phosphoglycerate; 2PG, 2-phosphoglycerate; PeP, phosphoenolpyruvate. Enzyme: PRK, phosphoribulokinase.

1.5 Overview of Research

The overall goal of this thesis is to gather additional evidence for photosynthesis and activity of the RuBisCO shunt in *Cuscuta*. *C. gronovii* in particular is considered to be

holoparasitic, but residual greening and an autotrophic mechanism such as the RuBisCO shunt could challenge that assumption, as well as cause a reconsideration of many other plants that are considered holoparasitic. This thesis comprises several different experiments with the goal of addressing various parts of this problem. Homology searches are used to identify putative homologs for important photosynthesis genes in *C. gronovii*, and differential expression analyses are used to examine the activity of this pathway across fruit and seedling development. Several other pathways are analyzed in this manner: chlorophyll synthesis, lipid synthesis (broadly, triacylglycerol and fatty acid synthesis pathways), the RuBisCO shunt, and the Calvin cycle. A ^{13}C stable isotope tracking experiment is used to indirectly measure the activity of RuBisCO, using isotope fractionation as a signal for RuBisCO activity in various parasite tissues. Finally, the internal anatomy of *C. gronovii* tissues is examined, including overall stem and vasculature organization, chlorophyll autofluorescence, and nutrient accumulation. This serves as a pilot for future *Cuscuta* anatomy studies. Overall, the results of this thesis show that the expression of photosynthesis genes is upregulated across fruit and seedling development, and that RuBisCO plays a role in building plant tissue, though the exact nature of that role is still unclear.

Chapter 2

Materials and Methods

2.1 Overview of Bioinformatic Methods and Gene Search

Data analysis was conducted using the public Galaxy Europe server, private servers on the PSU BX infrastructure, and on a personal computer. The putative functions of *C. gronovii* genes were determined with nucleotide BLAST reciprocal best hits (RBH) against the TAIR10.1 *Arabidopsis thaliana* genome (traditional blastn, 1e-05 e-value cutoff).

The *A. thaliana* genes involved in each pathway of interest—photosynthesis light reactions, RuBisCO shunt, chlorophyll synthesis, lipid synthesis, and Calvin cycle—were determined through different means. The Plant Metabolic Network's PlantCyc database was used to determine gene lists for the RuBisCO shunt, Calvin cycle, fatty acid synthesis (FA), and triacylglycerol (TAG) synthesis (Hawkins et al., 2021). Additional genes for TAG synthesis were determined from a review by Hölzl & Dörmann (2019), photosynthesis gene lists were determined from Tyagi & Gaur (2003), and chlorophyll synthesis gene lists were determined from Timilsena et al. (2023). A complete list of all genes of interest can be found in Appendix D.

All differential expression analyses were conducted in R using DESeq2 v1.40.2, and visualizations were made using the ggplot2 package. Detailed tool settings for the QuantSeq protocol and tool sources can be found in the Appendix, along with links to a Galaxy workflow.

2.2 mRNA Sequencing, Post-Processing, and Mapping

mRNA was extracted from 21 different *C. gronovii* tissues (Appendix A) by Paula Ralph and Juan Cerda in September 2022 using Macherey-Nagel Nucleospin RNA Plant kits. The RNA-seq libraries were prepared by the PSU Genomics Core using Lexogen's QuantSeq 3' mRNA-Seq FWD Library Prep Kit with UDI. All subsequent processing (trimming and mapping) was done as part of this thesis. Raw FASTQ reads were processed and analyzed according to the recommendations by Lexogen (Lexogen GmbH, 2018, 2024). Cutadapt v4.4 was used to remove adapter and poly-A sequences, and quality controls were performed using FastQC v0.12.1 and Qualimap v2.3. Post-processed reads were then mapped to the JDC1 *C. gronovii* genome using STAR v2.7.10b and quantified using the v0.3 annotation with HTSeq-count v2.0.5.

2.3 Genome Construction and Annotation Evaluation

The genome (JDC1) and annotations used in this project were constructed by Juan Cerda in 2022 and 2023, respectively (Cerda & dePamphilis, n.d.). The BRAKER pipeline was used by Juan Cerda to build the original gene models, and the untranslated regions (UTRs) were later added and modified to produce several versions of the annotation. The v0.1 annotation was produced with BRAKER, the v0.2 annotation added some UTRs using TransDecoder, and the v0.3 annotation—the most recent version as of this thesis—used PASA to extend UTRs. As QuantSeq sequencing focuses on the 3'-UTR region, the QuantSeq libraries were used to evaluate annotation quality. Annotation evaluation was completed as part of this thesis using HTSeq-count after read trimming and mapping (Appendix C).

2.4 Carbon Isotope Tracking

A ^{13}C-enriched urea solution was prepared and applied to plants following the general guidelines of Schmidt & Scrimgeour (2001): 2 $g*L^{-1}$ urea (Cambridge Isotope Labs CAS 58069-82-2) in DI water, and 2.5 mL Tween-20. Urea solution was stored at room temperature away from light.

A parent *C. gronovii* plant (strain MC3413) was germinated in April 2023, and allowed to spread over several tomato (*Solanum lycopersicum* introgressed line IL-8-1-1, described in Hegenauer et al., 2016) during Summer and Fall 2023. The parent plant began to flower in June and continued until senescence later in the fall. *Amaranthus tricolor* (from commercial seed packet by Botanical Interests) seeds were sown in September 2023, and week-old seedlings were repotted for treatment, for a total of 5 control plants and 5 treatment plants. The treatment plants were sprayed with 20 mL enriched urea solution for the first week. After this, *Cuscuta* cuttings were taken from the parent plant, placed in an Eppendorf tube with water, and left near each treated and untreated *Amaranthus* plant. During the process of *Cuscuta* attachment and growth, ^{13}C-enriched *Amaranthus* plants were treated with urea every other day. To limit contamination with *Cuscuta* cuttings, the largest leaves of each *Amaranthus* plant were painted with ^{13}C urea solution, and some solution was also applied to the roots of each plant. Treatment continued until Mid-November, and tissue was collected 10 days later. Only 3 of the 5 *Amaranthus* plants had successful attachments, and none of the 5 control (unenriched) plants had successful attachments.

The following tissues were collected from the 3 ^{13}C-urea treated plants: host (*Amaranthus*) leaf, parasite (*Cuscuta*) stem, parasite flower buds, and parasite fruits. The fruits

were also divided into seeds and surrounding tissue ("fruit cover" tissue, Fig. 3F). *Amaranthus* leaf and *Cuscuta* fruit covers were ground in a bead mill, but the remaining samples were either hand-ground (stem) or left whole to preserve material. Samples were prepared for isotopic analyses in 5 x 9 mm tin capsules, with approximately 2 mg of tissue per sample. All samples were packaged in a 96-well plate and sent for analyses at EcoCore Analytical Facility, Colorado State University. Data was analyzed in R using the lme4 and emmeans packages. A linear mixed-effects model using plant identity (plant 1 to 3) as a random effect was used, followed by ANOVA.

2.5 Staining, Sectioning, and Microscopy

All *C. gronovii* tissues were hand-sectioned with razor blades. Stem samples were prepared for viewing under brightfield microscope and stereomicroscope. Sections were stained with Toluidine Blue (TB) and Lugol KI for 10 seconds each, and with Nile red for 3 minutes. The Nile red solution was prepared according to recommendations in Steinberg (2009), with a stock solution of 10 mL DMSO and 4 mg Nile Red diluted to a 200-fold working solution. Nile red fluorescence in stem tissue was observed under stereomicroscope with green light.

Peduncle and seed tissues were prepared separately for chlorophyll autofluorescence analysis and lipid imaging, and peduncle tissue was stained with Nile Red for 30 seconds. Imaging was conducted on a Zeiss LSM 510 META confocal microscope. Chlorophyll autofluorescence was viewed with a 488 nm laser, HFT 405/488 and NFT 565 dichroic mirrors, and LP 420 and 650 long-pass filters. Nile red fluorescence was viewed with a 561 nm laser, HFT 458/514/561 and NFT 565 dichroic mirrors, and LP 420 and 575 long-pass filters.

Chapter 3

Results

3.1 Homology Search for Genes of Interest

Of the 30,291 features currently included in the *C. gronovii* v0.3 annotation, 15,616 (51.6%) found a RBH homolog in the TAIR10.1 *A. thaliana* genome. In contrast, 17,676 of the 27,562 (64.1%) *A. thaliana* genes found at least one RBH homolog. Most of the original genes of interest that were identified through literature searches found at least one homolog in *C. gronovii*, with over 90% of *A. thaliana* genes from the photosynthesis, RuBisCO shunt, chlorophyll synthesis, and fatty acid synthesis databases being represented at least once (Table 1).

Table 1. Summary of RBHs for *Arabidopsis* genes of interest.

V0.3 Annotation, Genes of Interest	
Photosynthesis genes:	44 of initial 46 genes, **95.7%**
RuBisCO shunt genes:	36 of initial 39 genes, **92.3%**
Chlorophyll synthesis genes:	25 of initial 27 genes, **92.6%**
Fatty acid synthesis:	44 of initial 46 genes, **95.7%**
Triacylglycerol synthesis:	44 of initial 57 genes, **77.2%**

Many genes in *C. gronovii* also showed a complex pattern of orthology with their *A. thaliana* counterparts (data not shown). An example is the genes cugr10192 and cugr30275, which both found an RBH with 4 different *Arabidopsis* genes (1 transferase and 3 different esterase/lipase/thioesterase genes), forming a potential 2:4 co-orthology relationship. Some genes have an even more complex pattern of potential orthology, such as cugr10006. This gene,

along with 4 other *Cuscuta* genes, forms a 5:3 co-orthology relationship with *Arabidopsis* genes, and also finds RBHs in 6 other *Arabidopsis* genes in addition to this.

3.2 Differential Expression Quality Control

The overall variation across the QuantSeq stages is shown using PCA plots (Fig. 5). Clustering is clear among some stages, such as all haustorial and floral stages clustering together, but some samples are found further than expected from their replicates. One starved seedling shoot sample (library 2.2.1, bioreplicate 4) is found close to two imbibed seed samples, while a different imbibed seed sample (library 1.3, bioreplicate 5) is found clustering with the starved seedling tissues). This suggests swapped samples, and these two samples (2.2.1_P4 and 1.3_P5) were removed for further analyses. Without these samples, greenness (and thus hypothetical photosynthetic activity) can be used to explain most of the variation seen in PC2 (Fig. 5B). Overall activity can also be used to explain the variation seen in PC1, with dormant stages (seeds and brown fruits) clustering together (Fig. 5C).

3.3 Fruit Gene Expression

The expression of photosynthesis genes across fruit development is shown in Fig. 6, where each of the 5 stages of fruit development (pre-meiotic flower, post-meiotic flower, open flower, green fruit, and brown fruit) is compared with normal stem tissue. Each of the fruit development stages (except for brown fruit) showed several genes that were significantly higher in expression than the stem base, shown by genes with a positive log2 fold-change (log2FC). Over the course of development (growing flowers and green fruit, Fig 6A-D), more genes

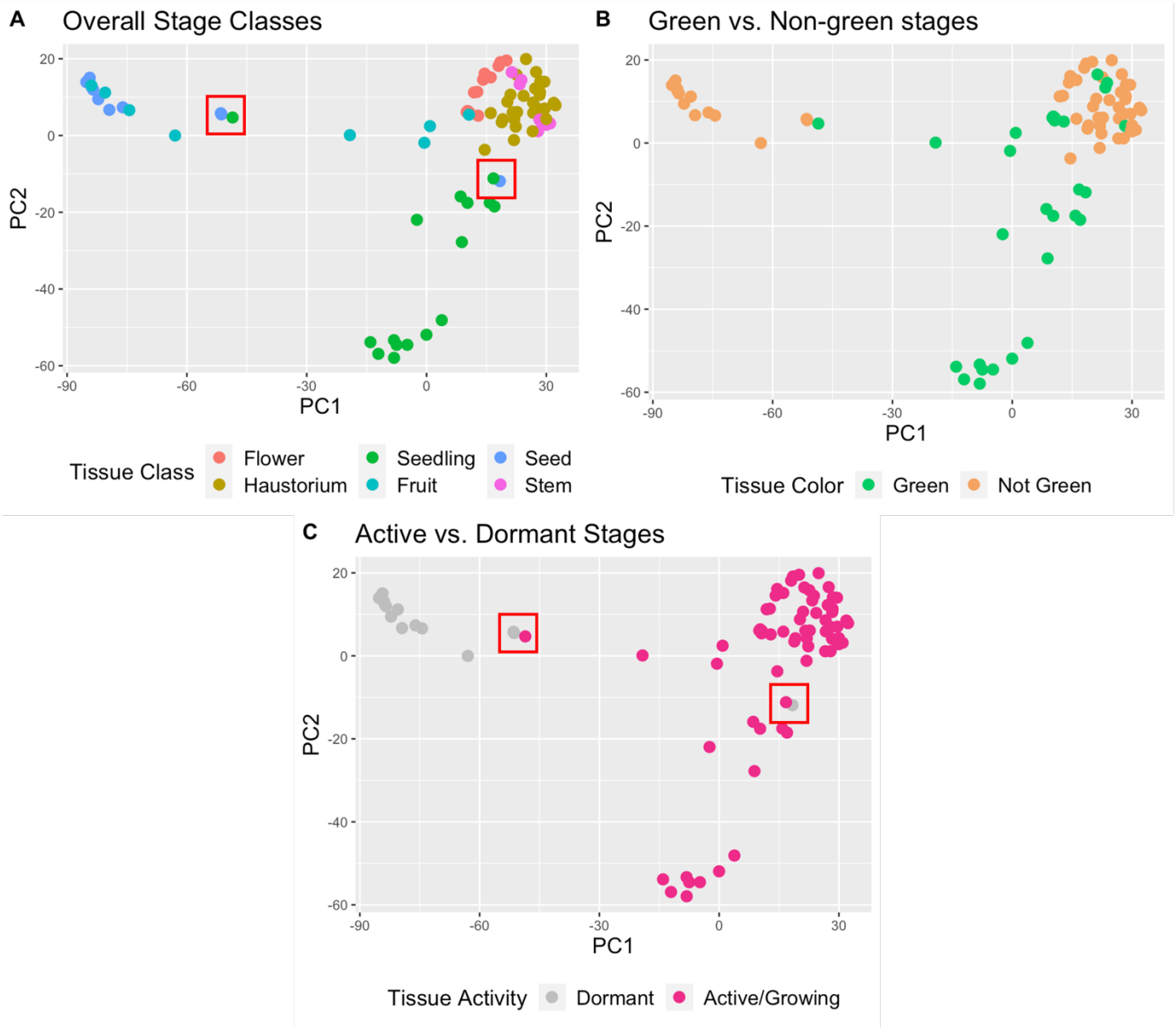

Figure 5. PCA plots of all QuantSeq stages. Stages are organized by overall tissue type (A), by greenness (B), or by general activity (C). Red boxes show samples that appear to be swapped.

become significantly different from stem base, though the level of expression does not change significantly. The average log2FC for these genes ranges from 0.84 (pre-meiotic flower) to 1.16 (green fruit) for a 1.8-fold to 2.2-fold increase in expression, respectively. The trend of increasing photosynthesis gene activity abruptly reverses in the brown fruit (Fig. 6E), with a number of photosynthesis genes being more highly expressed in the yellow stem base. The

average log2FC for these genes is -2.82, for a 7-fold increase in expression in stem tissue compared with brown fruit.

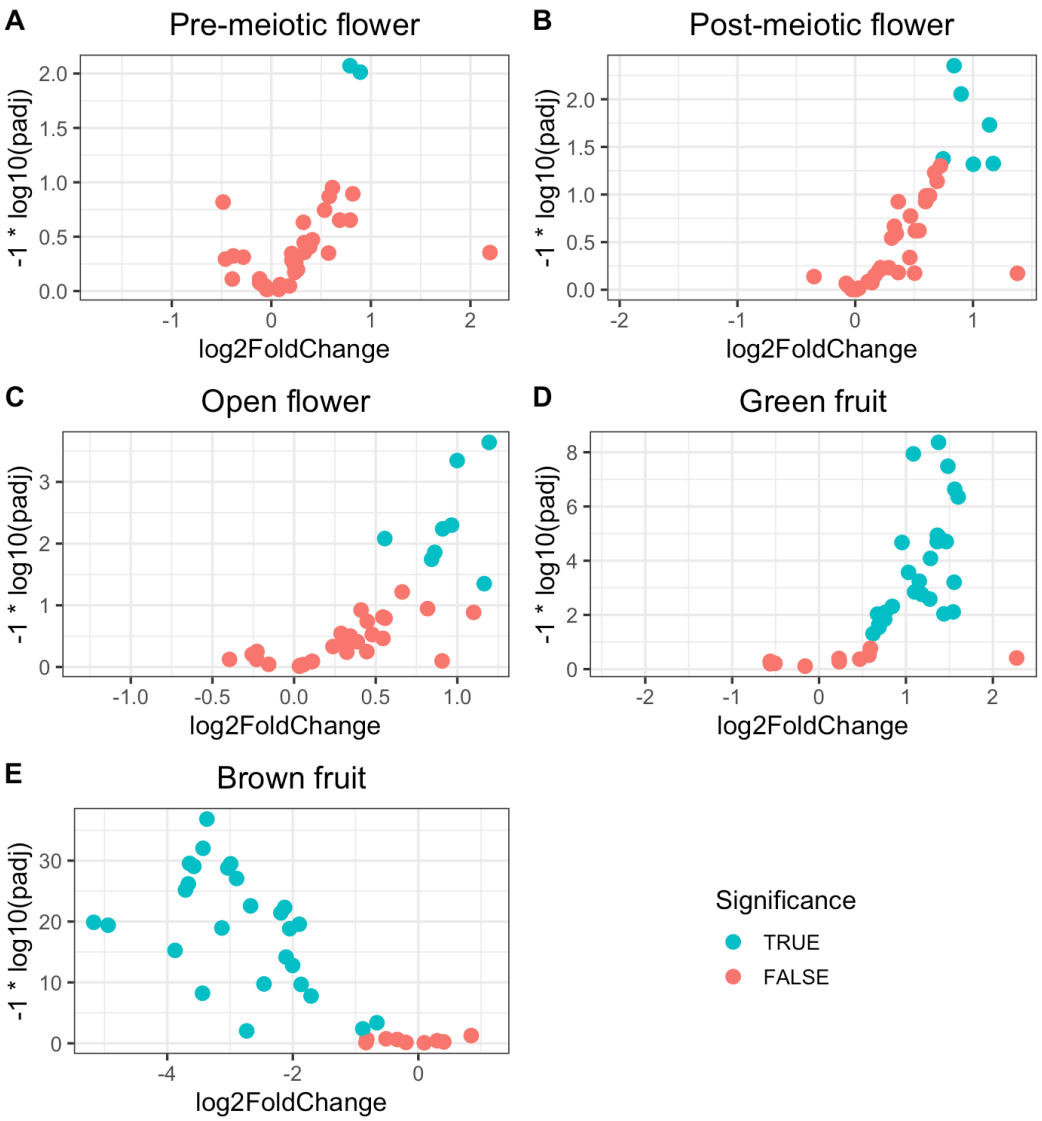

Figure 6. Expression of photosynthesis genes across fruit development. Volcano plots show the log2-transformed fold-change of each gene in relation to its adjusted p-value. Each tissue of interest is contrasted against base stem tissue (library 5.2), and positive log2FC values indicate upregulation of a gene in the contrast tissue.

A fruit development series is also useful to visualize changes in lipid synthesis (Fig. 7). There are no overarching patterns in the data—most of the genes appear to be down-regulated with respect to the tissue of interest, and thus up-regulated in the stem base. A few genes stand

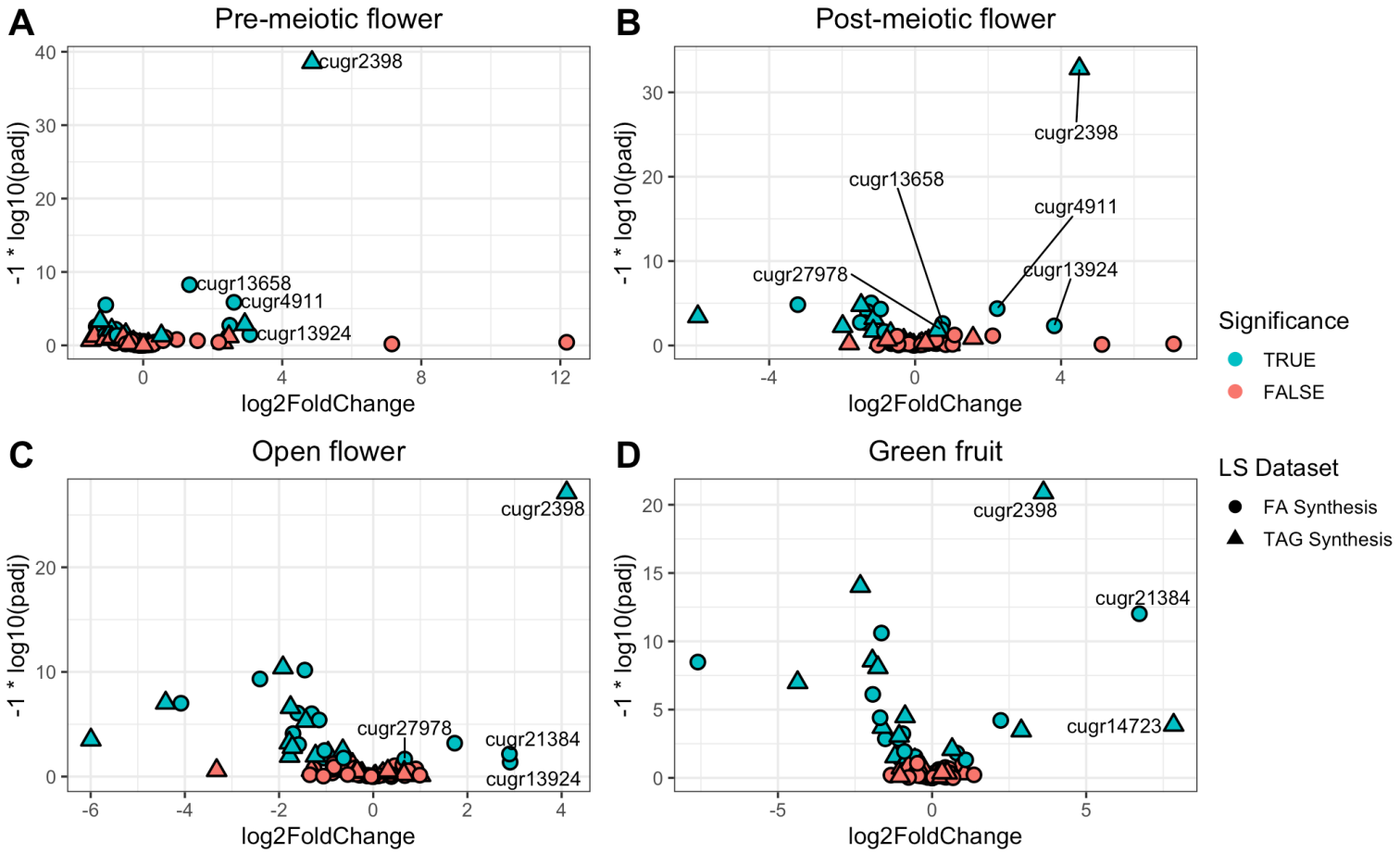

E

Gene	Average log2FC	Fold-change	Homologs	Database
cugr14723	7.84	228.80	AT3G49210, AT3G49200	TAG Synthesis
cugr21384	4.81	28.03	AT3G02610, AT3G02620, AT3G02630, AT5G16230, AT5G16240, FTM1, SSI2	FA Synthesis
cugr2398	4.27	19.30	AT5G12420, AT3G49200	TAG Synthesis
cugr13924	3.26	9.60	LACS8, LACS9	FA Synthesis
cugr4911	2.43	5.39	AT4G11030, LACS4, LACS1, LACS2, LACS3	FA Synthesis
cugr13658	1.04	2.06	AT1G10310	FA Synthesis
cugr27978	0.69	1.62	ACOS5	FA Synthesis

Figure 7. Expression of lipid synthesis genes across fruit development (A-D). The two pathways of interest, fatty acid synthesis and triacylglycerol synthesis, are shown. E, a table of particularly notable genes and their *Arabidopsis* homologs.

out with high expression in the tissues of interest (Fig. 7E). Cugr2398, which has a putative O-acyltransferase function (homolog of AT3G49200 and AT5G12420), is highly expressed across developing flowers and green fruits (average log2FC of 4.27, 19.3-fold increase). The single most highly expressed lipid synthesis gene in the green fruit (cugr14723) also has putative O-acyltransferase function (homolog of AT3G49210 and AT3G49200), with a ~230-fold increase relative to the stem base. A handful of genes also have high expression in the floral tissues, but no significant increase in the green fruit.

The genes of the RuBisCO shunt do not show any significant pattern in the fruit development series: a seemingly random set of genes is differentially expressed in each stage (Appendix E, Fig. 20). The one exception to this is cugr860, which is a homolog of RuBisCO small chain proteins (RBCS). This gene is overexpressed in the green fruit compared to stem base, with a log2FC of 1.16 (2.23-fold increase in expression).

3.3 Seedling Gene Expression: Photosynthesis and Chlorophyll Synthesis

Similar patterns of expression of photosynthesis (Fig. 8) and chlorophyll synthesis (Fig. 9) genes can be seen when comparing seedlings with base stem. With each dataset, a group of several genes (more in photosynthesis than in chlorophyll synthesis) are more highly expressed in the normal and starved seedlings than in stem tissue. However, when normal and starved seedlings are compared against one another, there is no significant pattern of gene expression in either chlorophyll synthesis or photosynthesis.

Using the photosynthesis dataset, the gene with the highest expression in both normal and starved seedlings is cugr10155, with putative cupredoxin/plastocyanin function (homolog of

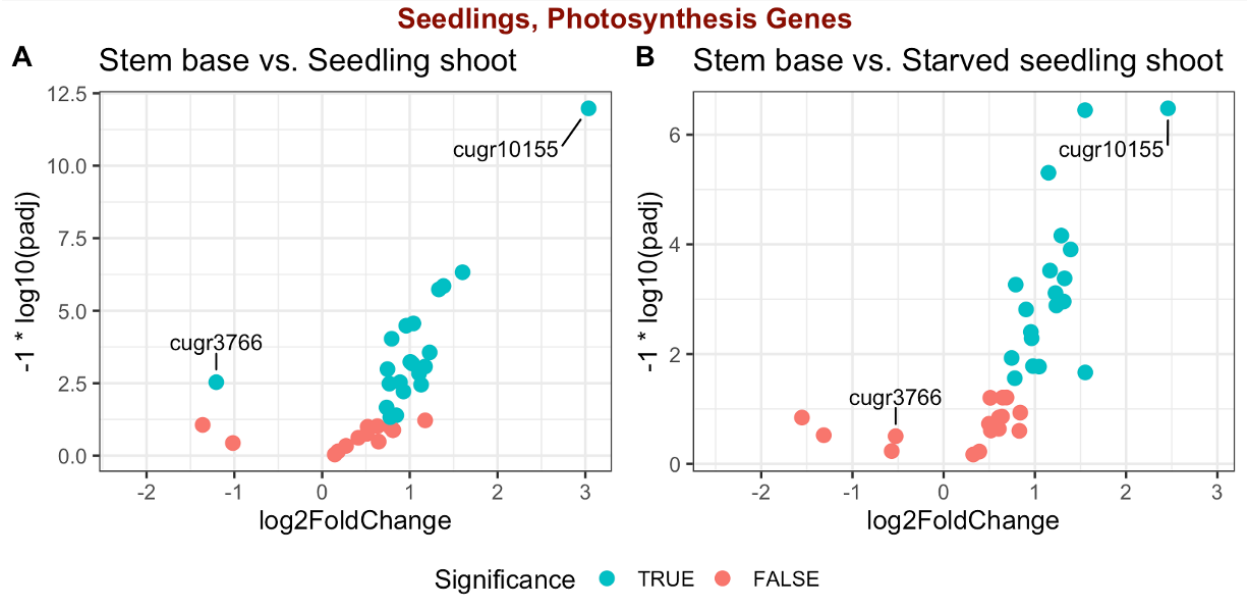

Figure 8. Volcano plots of photosynthesis genes, comparing normal (A) and starved (B) seedling shoots against stem base. The only gene with higher expression in stem base (A) is cugr3766, putative photosystem I subunit F (PSAF).

DRT112 and PETE1). The average log2FC for photosynthesis genes more highly expressed in the normal and starved seedlings is 1.12 (2.18-fold increase) and 1.20 (2.3-fold increase), respectively.

Based on the chlorophyll synthesis dataset, fewer genes are highly expressed in the seedling tissues, though still more than in stem base. Overall, the levels of expression for chlorophyll synthesis genes are similar across tissues. The average log2FC for chlorophyll synthesis genes more highly expressed in the normal and starved seedlings are 1.27 (2.41-fold increase) and 1.13 (2.19-fold increase), respectively, although the genes more highly expressed in the stem base have a similar log2FC of -1.23 (2.35-fold increase in stem tissues).

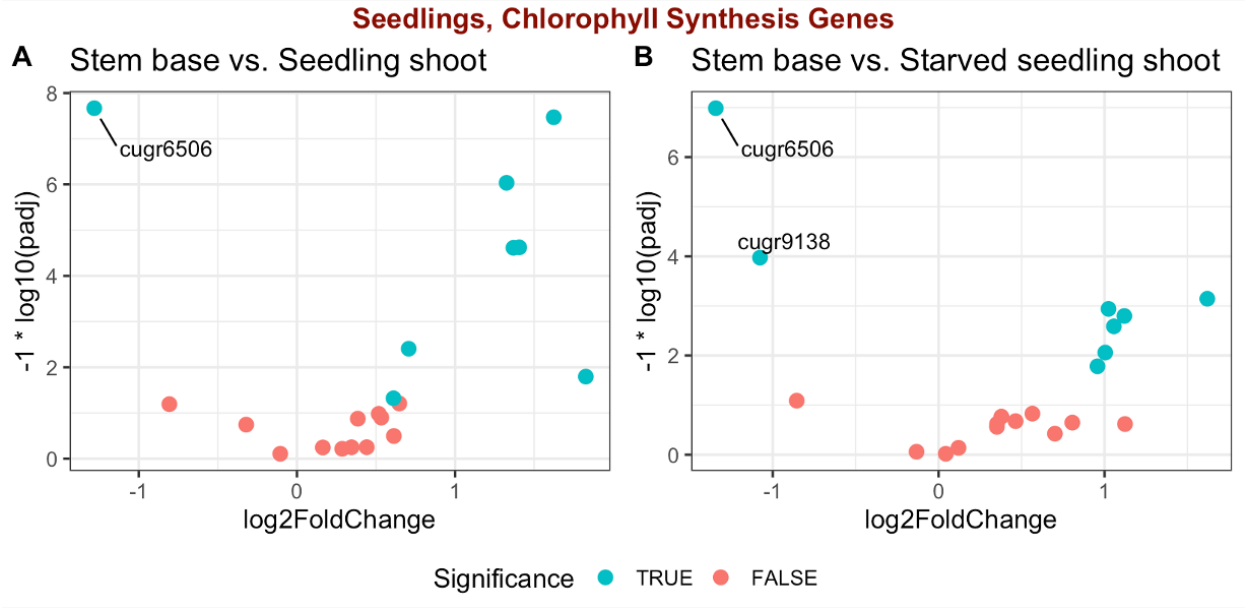

Figure 9. Volcano plots of chlorophyll synthesis genes, comparing normal (A) and starved (B) seedling shoots against stem base. The only genes with higher expression in stem base are cugr6506 (A, B), putative coproporphyrinogen oxidase (AT1G68220); and cugr9138, putative phytochromobilin synthase (AT3G09150).

3.4 Seedling Gene Expression: Lipid Synthesis and Calvin Cycle

The expression of lipid synthesis genes in seedlings follows an interesting pattern (Fig. 10, Table 2). There is very little difference in the expression of genes when comparing normal and starved shoots, with the only significant gene (cugr17876, putative acyl-CoA synthetase) having a negligible log2FC of 0.71 (1.64-fold increase). However, several TAG synthesis genes are overexpressed in the normal radicle compared to starved seedling. The only FA synthesis gene overexpressed in unstarved radicle tissue is cugr21383, which is a putative acyl carrier protein (log2FC of 1.51, 2.85-fold increase).

The expression of Calvin cycle genes in seedling radicle and shoot is shown in Fig. 11. In this case, the radicle and shoot show different patterns of expression depending on whether normal (Fig. 11A) and starved (Fig. 11B) tissues are compared. Starved seedling radicle shows

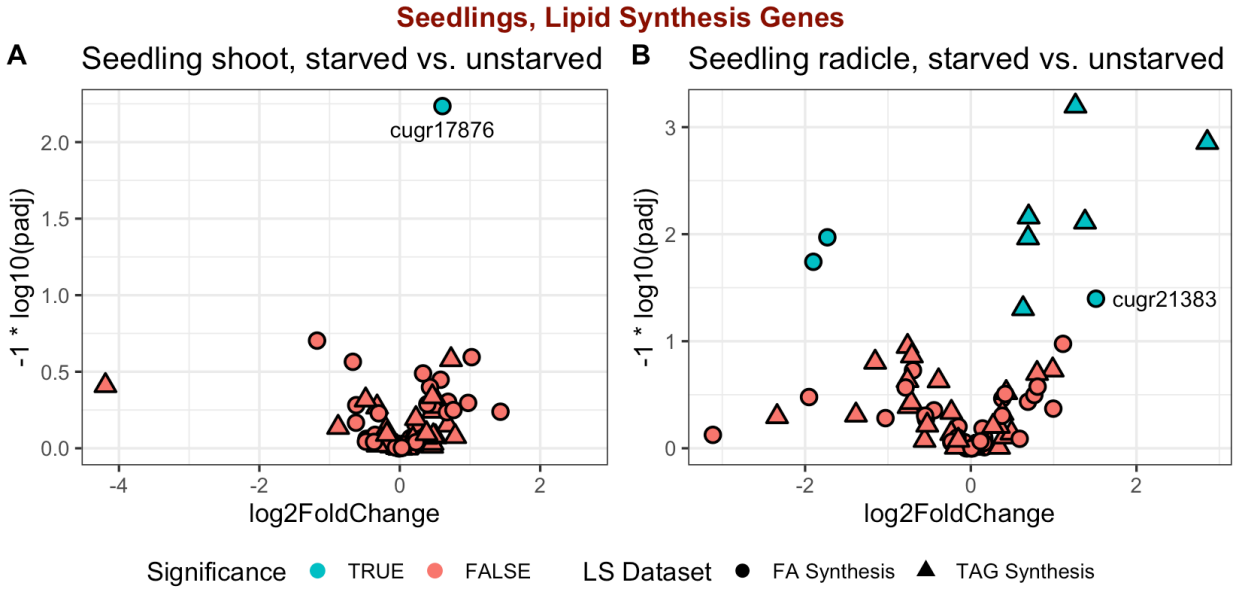

Figure 10. Volcano plots of lipid synthesis genes, comparing normal and starved seedling shoot (A) and radicle (B) tissue. The only significantly different gene in normal vs starved seedling shoot (A) is cugr17876. The only FA synthesis gene that is significantly upregulated in normal vs starved radicle (B) is cugr21383.

Table 2. Lipid synthesis genes overexpressed in normal vs. starved seedling radicle tissue (Fig. 10B).

Gene	Dataset	Putative function	Homologs
cugr9554	TAG Synthesis	O-acyl transferase	TAG1
cugr2874	TAG Synthesis	lecithin:cholesterol/phospholipid:DAG acyltransferase	AT3G44830, PDAT
cugr16118	TAG Synthesis	DAG acyltransferase	DGAT2
cugr19976	TAG Synthesis	fatty acyl-ACP thioesterase	FATA, FATB
cugr20538	TAG Synthesis	glycerol-3-phosphate/phospholipid acyltransferase	AT3G11325, GPAT5, GPAT7, GPAT4, GPAT3, GPAT1
cugr17110	TAG Synthesis	alpha/beta hydrolase	AT4G24160
cugr21383	FA Synthesis	stearoyl acyl carrier desaturase	AT3G02610, AT3G02620, AT3G02630, AT5G16230, AT5G16240, FTM1, SSI2

the upregulation of a number of different genes compared to starved seedling shoot, including two of the three genes upregulated in unstarved radicle. The Calvin cycle-exclusive genes phosphoribulokinase (PRK), RuBisCO (small chain subunit, RBCS), and sedoheptulose-1,7-

bisphosphatase (SBPase) are shown in the starved tissue comparison. PRK and SBPase were differentially expressed in the starved radicle but not in the unstarved radicle, and the RBCS gene cugr860 was not differentially expressed in any of the tissues compared. The average log2FC of genes differentially expressed in the shoot also decreases between starved and unstarved tissue: the average log2FC of unstarved shoot genes is 1.36 (2.56-fold increase), whereas the average log2FC of starved shoot genes is 1.12 (2.17-fold increase). The average log2FC of starved radicle genes is -1.44 (2.71-fold increase).

Also notable is the identity of the genes that are upregulated in starved and unstarved radicle tissue (Tables 3 and 4). The three genes that are upregulated in unstarved radicle (cugr10124, cugr1264, and cugr23358) are all also upregulated in the starved radicle—except for cugr10124, though it is a potential paralog of cugr25166. A few additional genes of varying functions are upregulated in the starved radicle, along with PRK and SBPase.

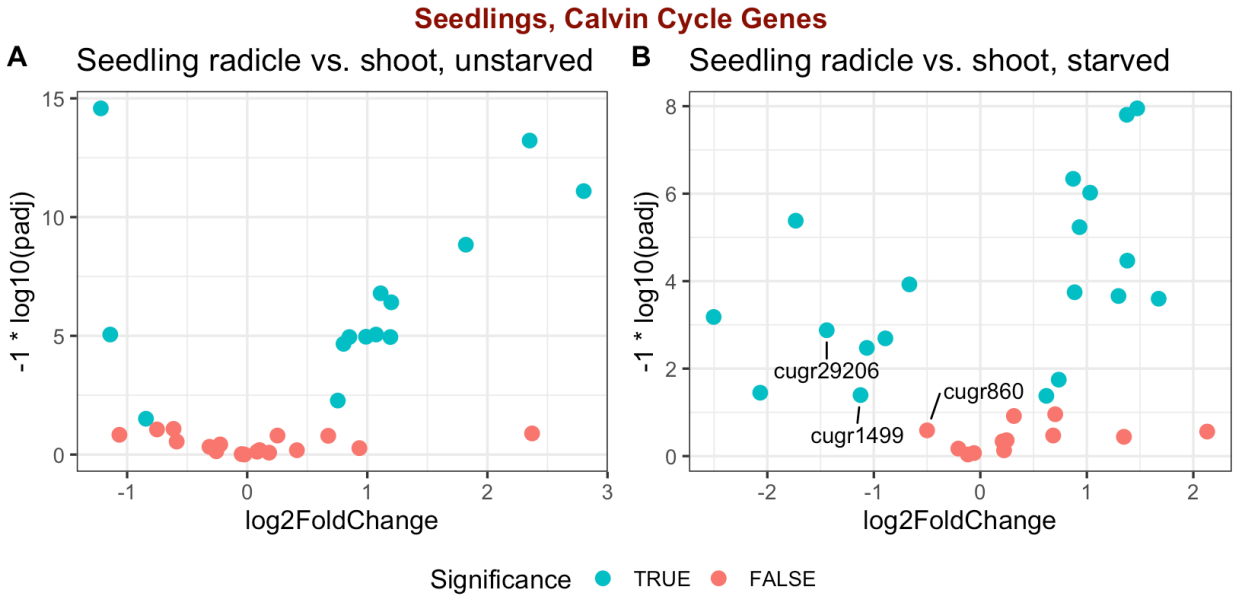

Figure 11. Volcano plots of Calvin cycle genes, comparing seedling radicle and shoot under normal (A) and starved (B) conditions. Notable genes include cugr29206 (homolog of PRK), cugr1499 (homolog of SBPase), and cugr860 (homolog of RBCS). None of these genes are differentially expressed in unstarved radicle/shoot (A).

Table 3. Differentially expressed Calvin cycle genes with higher expression in starved radicle (Fig. 11B)

Gene	Putative function	Homologs	log2FC (–fold increase)
cugr25166	G3P dehydrogenase (C2)	AT1G13440	-2.07 (4.19)
cugr1264	Aldolase-type TIM barrel family protein	AT1G63290, AT3G01850	-0.67 (1.59)
cugr23358	D-ribulose-5-phosphate-3-epimerase	AT5G61410	-1.13 (2.18)
cugr29206	phosphoribulokinase	AT1G32060	-2.5 (5.67)
cugr1499	sedoheptulose-1,7-bisphosphatase	AT3G55800	-0.89 (1.86)
cugr3267	sedoheptulose-1,7-bisphosphatase	AT3G55800	-1.73 (3.32)
cugr10198	phosphoglycerate mutase	AT1G08940	-1.44 (2.72)
cugr21475	Inositol monophosphatase	AT1G43670	-1.07 (2.09)

Table 4. Differentially expressed Calvin cycle genes with higher expression in unstarved radicle (Fig. 11A)

Gene	Putative function	Homologs	log2FC (–fold increase)
cugr10124	G3P dehydrogenase (A, C2)	AT1G13440, AT1G12900	-0.84 (1.79)
cugr1264	Aldolase-type TIM barrel family protein	AT1G63290, AT3G01850	-1.22 (2.33)
cugr23358	D-ribulose-5-phosphate-3-epimerase	AT5G61410	-1.14 (2.2)

3.4 Isotope Tracking Results

The average $\delta^{13}C$ values for all tissues of interest are shown in Fig. 12 along with respective confidence intervals. Seed, flower, and fruit cover tissues are all significantly different from stem tissue, but not from each other. All tissues except for fruit cover had 15 samples spread across 3 plants. Limited material resulted in only 3 samples for fruit cover, of which one (from plant 2) was removed because of low mass and measurement quality. The remaining tissues were spread evenly across each plant (5 per plant, total of 15) except for seeds, which were distributed according to material availability: 6 seeds from plant 1, 2 seeds from plant 2, and 7 seeds from plant 3. *Amaranth* host leaf tissue (2 samples per plant, 6 total), which was removed from these results due to incorrect sampling, had an average $\delta^{13}C$ of -9.21. Detailed statistics are shown in Table 5.

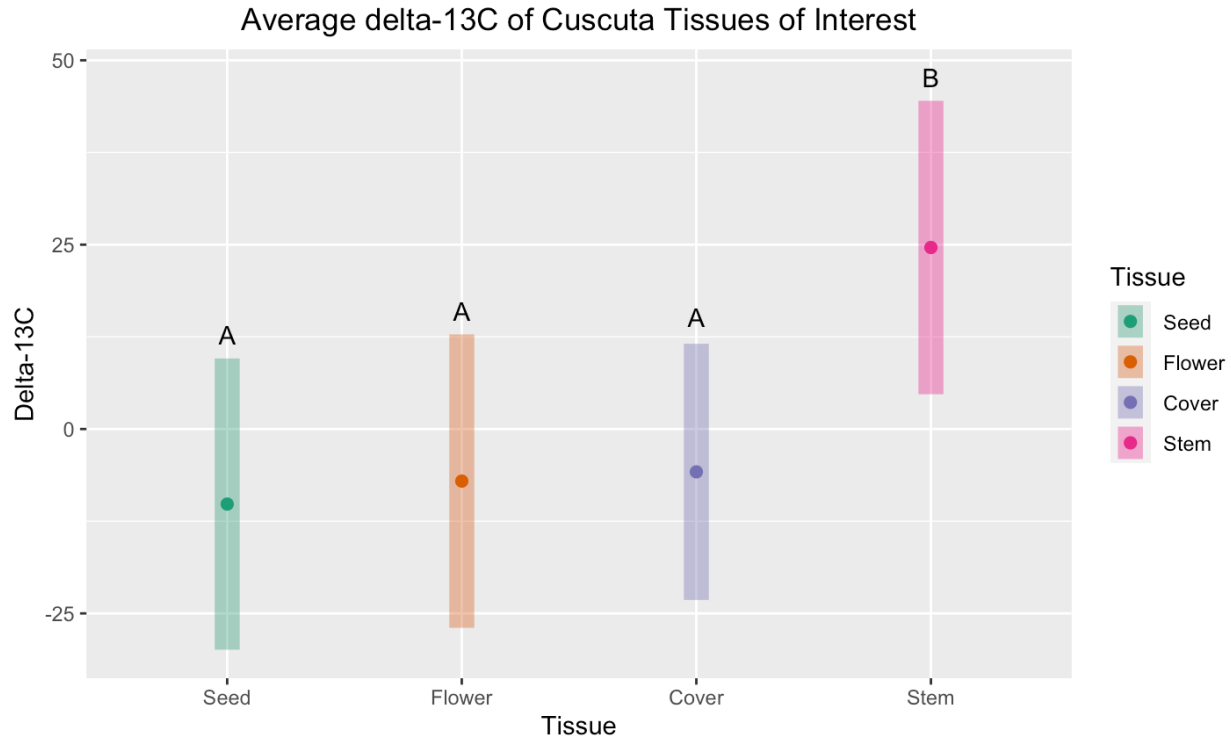

Figure 12. Results of the ^{13}C tracking experiment. Average $\delta^{13}C$ of each tissue is shown with confidence intervals. Significance: <0.0001 for all A–B.

Table 5. δ13C statistics for each tissue, as well as significance values for comparisons against stem tissue.

Tissue	# of samples	Mean	St. Error	Lower CI	Upper CI	p-value vs. Stem
Cover	2	-5.81	7.64	-23.18	11.57	6.46e-05
Flower	15	-7.06	5.46	-26.96	12.83	1.59e-12
Seed	15	-10.17	5.49	-29.92	9.57	9.50e-13
Stem	15	24.62	5.46	4.72	44.51	—

3.5 Microscopy Results

Some primary structural features of *C. gronovii* stems are shown in Fig. 13. The outer cuticle and epidermis are relatively thin but are clearly lignified, as shown by a dark blue TB stain (Fig. 13C) and strong fluorescence of Nile red (Fig. 13E). The outer cortex layer is also lignified and becomes more pectin-rich in inner layers. Some orange pigmentation is also visible near the epidermis and the center of the stem. Small vascular bundles are clearly visible in the inner layers, with small tracheary elements stained blue by TB (and visible with Nile red fluorescence). Below the tracheary elements are possible protoxylem cavities (lacunae), and above are phloem tissues with clearly distinguishable sieve-tube elements and companion cells. Phloem fibers and other specialized support tissues within the stem are not apparent and may be absent. Amyloplasts are also visible in both stem and peduncle tissues (Fig. 14). Amyloplasts in stems are distributed somewhat evenly among the non-lignified cells of the inner cortex and pith. They vary widely in size in both tissues, with large and small granules present in adjacent cells and sometimes even within the same cell. The optical section thickness for Fig. 14C was 1.8 μm.

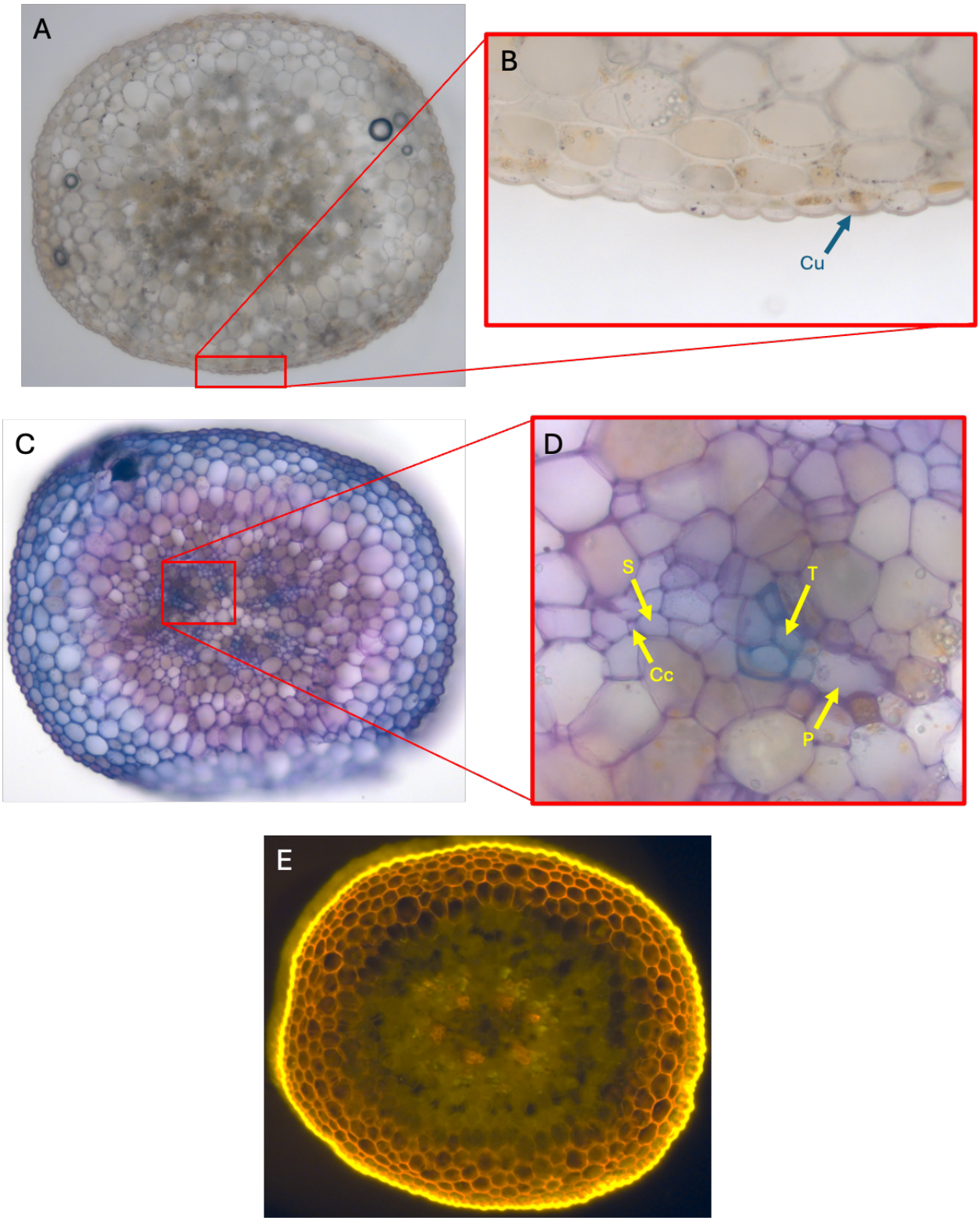

Figure 13. Major structural features in *C. gronovii* stem sections. Unstained tissue: (A) overall section (10x) and (B) detail of the outer cuticle showing some light orange pigmentation (40x). Toluidine blue stain: (C) overall section (10x) showing lignified outer tissue and (D) detail of a vascular bundle (40x). Nile red stain (E): overall section (10x) showing very bright epidermis. Details: Cu, cuticle; S, phloem sieve-tube element; Cc, companion cell; T, xylem tracheary element; P, protoxylem cavity.

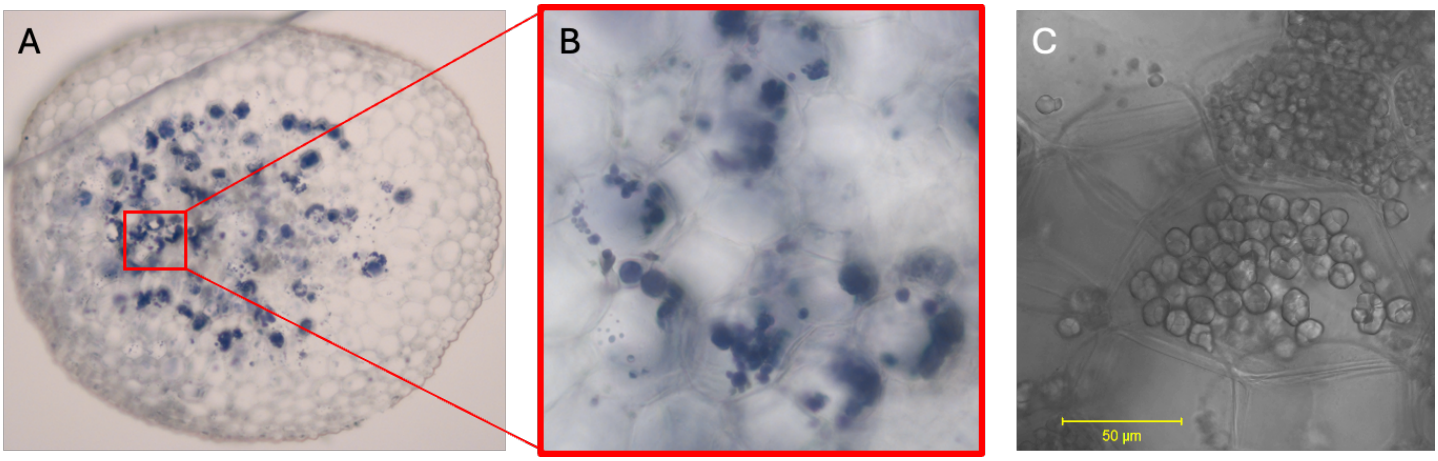

Figure 14. Amyloplast grains in *C. gronovii* stem. (A) Overall section stained with Lugol (10x). (B) Widely varying amyloplast sizes (Lugol, 40x). (C) Details of individual amyloplasts in peduncle tissue using confocal microscope (unstained).

Chlorophyll autofluorescence and Nile red fluorescence are examined in Figs. 15 and 16. Fig. 15 shows fluorescence along the outside edge of a green *C. gronovii* seed and a clear emission peak at ~675 nm for that fluorescence. Individual chloroplasts are not clearly visible with this resolution—optical section thicknesses were 3.0 µm (A-B) and 20.7 µm (C-E)—but fluorescence is visibly concentrated near the edges of the seed. Peduncle tissue stained with Nile red was examined for fluorescence and revealed some interesting anatomical features (Fig. 16). Large globules (Fig. 16A, features 2 and 3) were visible near the outer edge of the section, and each produced identical emission peaks at ~665 nm. Adjacent to the globules, another fluorescent object (Fig. 16A, feature 1) produced a different (but equally intense) emission peak at ~675 nm. Again, individual chloroplasts are not clearly visible. The optical section thicknesses of Fig. 16 images were 3.1 µm (A-B) and 1.8 µm (C-E).

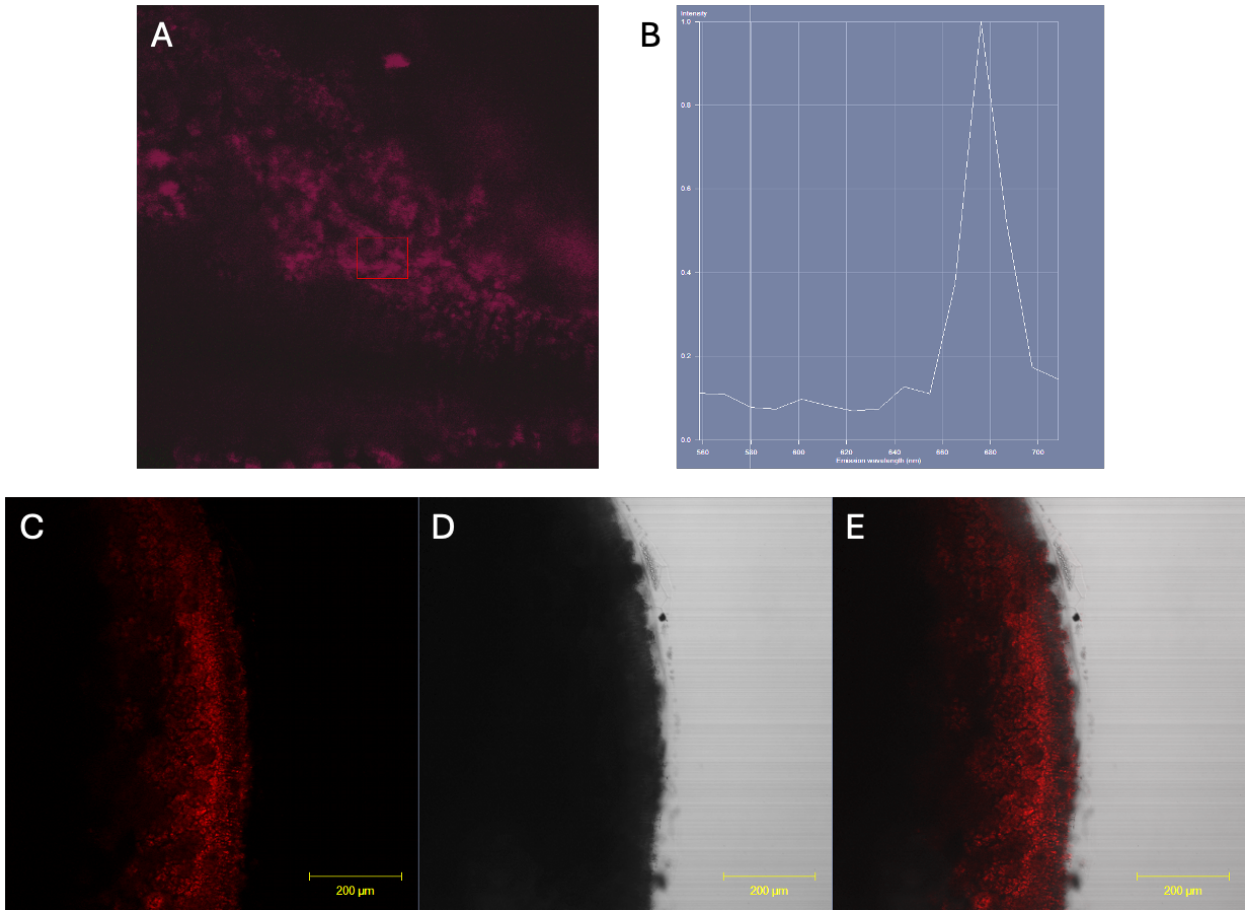

Figure 15. Chlorophyll autofluorescence in *C. gronovii* green seed, using 488 nm laser. Lambda scan of fluorescent area (A), showing a peak of emission at ~675 nm (B). Channel views (C-E) showing fluorescence in the outer layers of a seed.

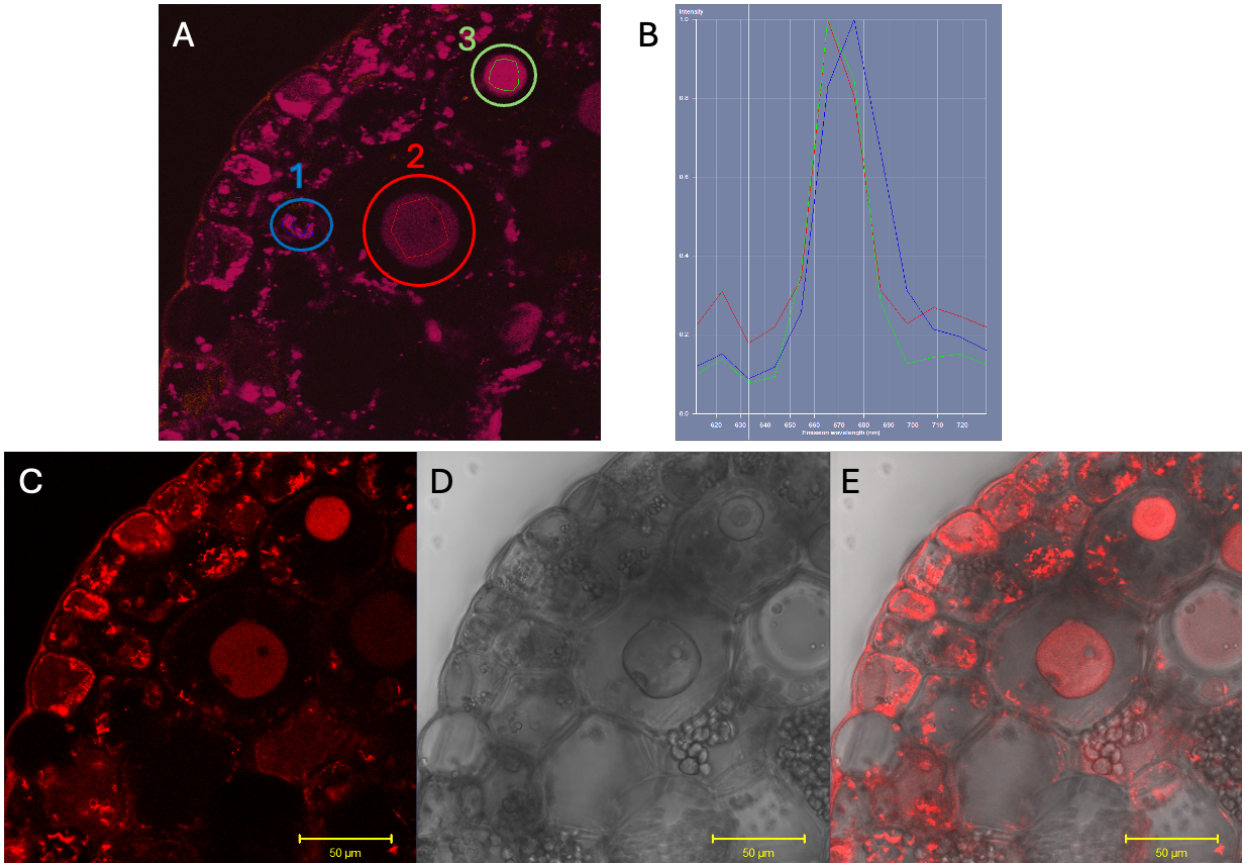

Figure 16. Nile red and potential chlorophyll fluorescence in *C. gronovii* peduncle, using 561 nm laser. Lambda scan of fluorescent area (A) and emission peaks for each area of interest (B). Channel views (C-E) showing fluorescence in the epidermis and surrounding tissues, and in large globules.

Chapter 4

Discussion

4.1 Homology and Gene Maintenance in *C. gronovii*

RBH is a well-established method to identify orthologous genes in different organisms and is extremely practical for its speed and accuracy, particularly when using reliable programs such as BLAST (Kristensen et al., 2011). A BLAST-based RBH analysis was extremely useful to quickly identify putative gene functions in *C. gronovii*. However, RBH produces a simple table of one-to-one matches, which can complicate the process of determining orthologous, co-orthologous, and paralogous relationships between genes. Many *C. gronovii* genes had complex many-to-many relationships, and as such the putative function of genes was based on only one of the potential matches with *A. thaliana*. The ideal method for establishing orthology relationships would be phylogenetic trees of gene families, but these are much more time-consuming and complex, as well as computationally intensive (Kristensen et al., 2011). Such an analysis is beyond the scope of this thesis but would be necessary for more in-depth analyses of gene evolution in *Cuscuta*. Additional functional annotation analyses, such as Gene Ontology (GO), would also be necessary to get a full picture of gene function.

C. gronovii shows a high level of gene maintenance for the pathways of interest, most notably in the genes of photosynthesis and chlorophyll synthesis (Table 1). Overall, homologs for over 90% of the *Arabidopsis* genes of interest for each pathway were identified in *C. gronovii*. Additional analysis may be necessary to determine whether any of these genes appear to be pseudogenes, and whether the existing genes could hypothetically be assembled into fully

functional pathways. Genes for the RuBisCO shunt were also highly maintained, but this is less notable because these genes are important for universal pathways such as glycolysis and pentose phosphate. An interesting exception to this is cugr860, which is the only homolog for RBCS found in *C. gronovii*. In contrast, 4 different RBCS genes are found in the *A. thaliana* genome, and each of these had only one RBH with cugr860.

Interestingly, only 77% of the genes in the TAG synthesis pathway were found in *C. gronovii*. Of these, most missing genes were O-acyltransferase WSD1-like proteins (8 of 13 missing). The most notable mising gene is a fatty acid exporter, FAX1, which is normally involved in transporting fatty acids out of the plastid for assembly into TAGs and other lipid molecules (N. Li et al., 2015). In *Arabidopsis*, this gene is essential for seed filling and pollen development, and the absence of this gene in *C. gronovii* suggests that some other mechanism must replace it to fulfil these functions (N. Li et al., 2015).

4.2 Photosynthesis Gene Expression

The most notable result from differential expression analysis is the gradual increase in photosynthesis gene expression visible across fruit development (Fig. 6). This clearly indicates the ramping up of photosynthetic activity as flowers mature, concurrent with the greening of fruits. While qRT-PCR would be necessary for more fine-grained analysis of changes in gene activity over time, this result provides strong early evidence for important photosynthetic activity during fruit development in a plant that is typically considered entirely holoparasitic. However, the activity of photosynthesis genes is not correlated with the activity of chlorophyll synthesis genes in fruits (as shown in Appendix E, Fig. 24). The results for chlorophyll synthesis suggest

that these genes are expressed in a fairly uniform way across all floral, stem, and green fruit tissues. It is worth noting that even in green fruits—the most photosynthetically active tissue, with 26 differentially expressed photosynthesis genes when compared to stem base—the average log2FC was only 1.16, for a 2.2-fold increase in expression. Fruits clearly have increased expression of photosynthesis, but there may also be some residual photosynthetic and chlorophyll synthesis activity in *C. gronovii* stems—though it is insufficient for survival away from a host.

Seedling tissues show a similar pattern of photosynthesis gene expression: both normal and starved seedlings show upregulation of photosynthesis compared to stem base (Fig. 8). This supports the hypothesis that low levels of photosynthesis may be important in keeping seedlings alive as they search for a host. However, there is no evidence from these data that starved seedlings—seedlings left without a host for 5 days—show any more photosynthetic gene expression than unstarved seedlings. Nor is there a clear difference between radicle and shoot tissues, though the radicle often dries up before the shoot apex and likely contributes less to seedling survival after germination. Seedling tissues differ from fruit tissues in that they show rather more expression of chlorophyll synthesis genes when compared to the stem base. A more in-depth examination of the genes involved and their respective roles would be necessary to draw further conclusions, but this suggests that seedlings use a different set of chlorophyll pigments than fruits and stems.

4.3 Lipid Synthesis Gene Expression

Unlike photosynthesis, there is no clear pattern of lipid synthesis in fruits, though this is likely due to an overabundance of genes of interest. Individual genes (such as cugr2398, fig. 7) show interesting patterns of expression, and resolving their potential roles in fruit development would require extensive searches of the literature and expression databases, such as ePlant (Waese et al., 2017). It is also difficult to link lipid synthesis expression directly to photosynthesis, though it is clear that some individual genes are exclusively upregulated in fruits. However, this is not enough to determine whether lipid synthesis in general is significantly upregulated in the fruits.

The pattern of lipid synthesis expression seen in seedlings has interesting implications for radicle function. Normal, unstarved radicle tissues show overexpression of a handful of TAG synthesis genes. These genes have a range of putative functions, but most are acyltransferases (Table 2). These genes are important for the remodeling of TAG molecules, and for the editing of FAs before addition onto TAG molecules (Chapman & Ohlrogge, 2012). The activity of these genes concurs with what is known about the organization of lipids in *Cuscuta* seeds. Martinčová et al. (2019) observed that oil droplets were concentrated around the hilum of *C. europaea* and *C. monogyna* seeds, suggesting that the radicle uses the energy from these deposits to push through the seed coat during germination. In-depth homology studies would be necessary to confirm the function of these *C. gronovii* proteins, but their putative functions appear similar to genes known to be involved in TAG catabolism in *Arabidopsis* (e.g., acyltransferases and thioesterases in early seedling growth: Cai et al., 2020; Y. Li et al., 2019). The only FA synthesis gene overexpressed in unstarved radicle tissue is a putative stearoyl-acyl carrier desaturase, which in *Arabidopsis* is

important for FA synthesis and cuticle formation during embryo development, thus its role in early *Cuscuta* seedlings is unclear (Kazaz et al., 2020).

This same pattern of expression is not seen in starved tissue, but this is likely because seedling radicles dry up after a few days of growth and should not require much energy after emerging from the seed.

4.4 Calvin Cycle Gene Expression

The changes in Calvin cycle gene expression between starved and unstarved seedling shoot/radicle suggests that the Calvin cycle is upregulated somewhat in starved tissue. This is somewhat contrary to expectations because the seedling radicle usually dries out before the shoot after several days of growth. However, this upregulation of the Calvin cycle could be used, after lipid and starch stores have run out, to generate a small amount of energy as a last-ditch effort to find a host. This could also indicate that the localization of the Calvin cycle shifts towards the radicle in an attempt to keep it alive for longer, but more detailed studies would be necessary to confirm this. Subsequent experiments should also take care to separate the starvation (greening) response from the desiccation response, which could confound gene expression results in the radicle.

The identity of the relevant genes is also suggestive of a potential shift in function (Tables 3 and 4). Glyceraldehyde-3-phosphate dehydrogenase (GAPDH) is an enzyme important in both glycolysis and the Calvin cycle, though different genes are responsible for each function: GAPC genes (glycolysis-specific) and GAPA/B (subunits of the Calvin cycle-specific GAPDH) (Muñoz-Bertomeu et al., 2009; Simkin et al., 2023). The GAPDH-related gene that is

upregulated in unstarved radicle, cugr10124, is a potential homolog for both GAPC and GAPA genes, so it is unclear whether glycolysis of the Calvin cycle is prioritized in this tissue. In starved tissue, however, cugr25166 is upregulated instead, which is a homolog of only GAPC. This suggests that glycolysis is upregulated in starved radicle tissue along with other enzymes of the Calvin cycle.

Outside of starved tissue, there is clear evidence of some Calvin cycle upregulation in the normal, unstarved seedling shoot. This, in addition to the fact that all of the genes necessary for the Calvin cycle (including the unique genes RuBisCO, PRK, and SBPase) are conserved in *C. gronovii*, is an additional signal that *C. gronovii* maintains some autotrophic ability at some points during its development. Interestingly, various Calvin cycle genes were also upregulated across fruit development and in stem tissues, suggesting that the Calvin cycle is active at a low level throughout the mature plant (Appendix E, Fig. 26).

4.5 Stable Carbon Isotope Tracking

The results of the ^{13}C tracking experiment suggest different rates of ^{13}C accumulation across different *C. gronovii* tissues grown on a ^{13}C-enriched host. The most notable result is that, as hypothesized, green seeds show very low ^{13}C accumulation (negative $\delta^{13}C$), which suggests that RuBisCO is indeed involved in carbon fixation in those tissues, and that the products of that fixation are used to build seed tissues. It is unclear from this experiment whether storage lipids and starches within the seed are also derived from RuBisCO-fixed carbon, and additional fine-grained experiments (such as lipid and starch extractions) would be necessary to resolve this. Interestingly, flower and fruit cover tissues also show this negative $\delta^{13}C$, which suggests that

RuBisCO is involved in constructing these tissues as well. Peduncles turn green soon after they begin to grow from the stem, so all floral structures may be in some way dependent on RuBisCO activity within *C. gronovii*, instead of receiving all their carbon from the host. Again, further experiments are necessary to determine whether the RuBisCO shunt or Calvin cycle are used in meaningful amounts during development.

It is also worth noting the significant limitations of this experiment. Firstly, the

Table 6. *Amaranthus tricolor* enrichment test results. One *Amaranthus* plant was treated with ^{13}C-enriched urea every day for 1 week, then 1 leaf of new growth was harvested 2 weeks later. Non-enriched leaf was harvested before treatment.

Sample	δ13C
Pre-treatment leaf 1.1	-17.93
Pre-treatment leaf 1.2	-17.99
Pre-treatment leaf 1.3	-18.00
Enriched leaf 1.1	125.08
Enriched leaf 1.2	124.08
Enriched leaf 1.3	122.27

Amaranthus host tissue showed no enrichment despite being grown with ^{13}C-urea treatment. It is reasonable to assume that the treatment was successful because *Cuscuta* stem tissues are enriched, but the *Amaranthus* leaves do not reflect this and thus the results are not entirely reliable. A previous test of the enrichment method demonstrated that *Am. tricolor* leaves do show significant enrichment after only a week of treatment (Table 6), but only new growth is expected to show this enrichment. Old growth was erroneously collected from the ^{13}C-urea treated *Amaranthus* plants along with the *Cuscuta* tissues, and so a future experiment should involve careful tracking of tissue ages relative to urea treatment to ensure that young, enriched *Amaranthus* tissue is collected. This, along with a change in treatment method (for example, treating only leaves), would increase confidence that any ^{13}C in *Cuscuta* must have come from

the *Amaranthus*. Using the data presented here, there is still a possibility that the ^{13}C found in *Cuscuta* may be from contamination left behind on the *Amaranthus* leaves, and there is no way to directly relate enrichment between parasite and host. Sampling was also particularly limited for fruit cover tissues, as the samples from only 2 plants had enough material to get accurate measurements.

4.6 Structural Features and Nutrient Allocation in *C. gronovii*

Microscopy of *C. gronovii* tissues was originally intended to solely examine nutrient localization, but the results show several interesting structural features. First and foremost, the heavily lignified epidermis and cuticle are visible on *Cuscuta* stems, along with some light orange pigmentation throughout the section that may be from chromoplasts (Fig. 13). This pigmentation is visible throughout the section, though this may be due to leaking of pigment or movement of chromoplasts after the section was made. This pigment (likely a carotenoid) is the source of *C. gronovii*'s notable orange color. Lignification is also visible in the outer layers of ground tissue (about half of the cortex), and there is a clear transition to pectin-rich cell walls.

The organization of vascular bundles is rather abnormal (Fig. 13): a few are scattered separately around the rough middle of the stem, and they contain a few small tracheary elements below phloem tissue. A small cavity (presumed to be an intercellular space due to its uneven border with neighboring cells) is visible below each tracheary element. This is likely a ruptured protoxylem vessel, which provided water flow during early development but was torn apart by surrounding cells as they grew, to be eventually replaced by the mature metaxylem tissue now visible (Protoxylem formation is described in Kubo et al., 2005). This organization of vascular

bundles, which can be seen in other *Cuscuta* species, is extremely different in species of *Ipomoea* (Fig. 17). *Cuscuta* lacks the uninterrupted ring of vasculature seen in *I. hederifolia*, and the tracheary elements are notably much smaller. There are also no lignified phloem structural elements visible (such as phloem fibers). This chaotic vasculature may be beneficial in a parasitic plant due to the extreme reorganization that is required during haustoria development. Small, thin-walled tracheary elements may also be useful for improving flexibility and taxis ability,

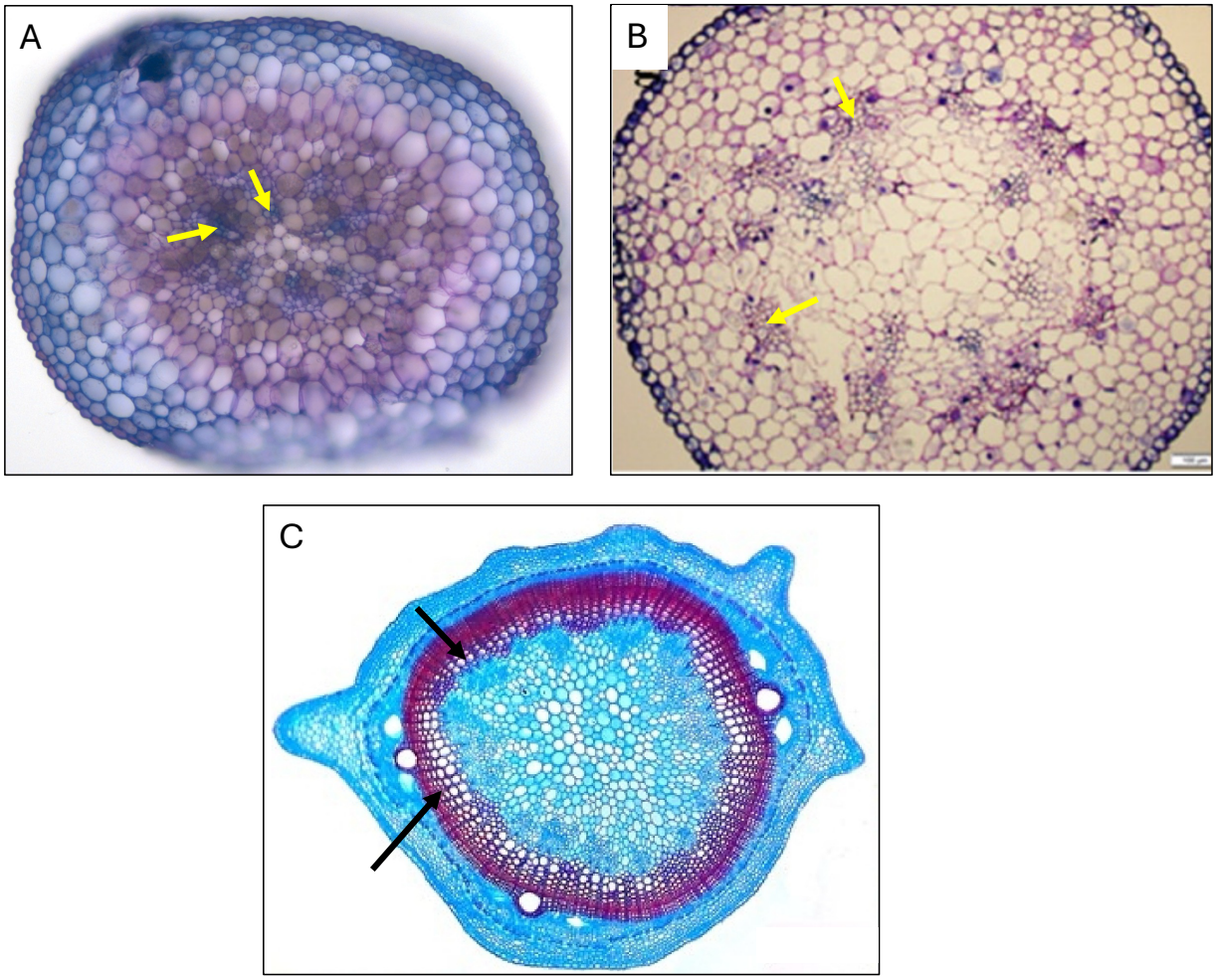

Figure 17. Comparison of vasculature in *Cuscuta* and *Ipomoea* stems. (A) *C. gronovii* and (B) *C. japonica* (Furuhashi et al., 2014) stems show a loose organization of small vascular bundles scattered around the pith, with small tracheary elements. (C) *I. hederifolia* (Santos et al., 2023) shows a complete, unbroken vascular cylinder surrounding the pith, with large vessel elements and a clear separation of xylem and phloem tissues. Arrows point to vascular structures.

which is important for twining and attaching to hosts. Amyloplasts are also present in stem and peduncle tissue, showing that both of these tissues are important for nutrient storage. Peduncle tissue was not observed with Lugol stain, but confocal images suggest that amyloplasts may be more densely packed in this tissue than in stems, which would give developing flowers and fruits easy access to nutrients as they develop.

Tests for chlorophyll autofluorescence show that this pigment is likely present in seeds. The peak emission for *C. gronovii* seeds under 488 nm excitation was ~675 nm, which is within the range of accepted literature values for chlorophyll *a* fluorescence (Taniguchi & Lindsey, 2021). Chlorophyll *b* is expected to fluoresce from ~645-660 nm, so the presence of chlorophyll *b* is less obvious (Taniguchi & Lindsey, 2021). A small peak at ~645 nm (Fig. 15B) suggests a small amount of chlorophyll *b* fluorescence, but more detailed analyses would be necessary to characterize the exact pigments present and their concentrations. The peduncle tissue analyzed for Nile red fluorescence also shows some possible chlorophyll autofluorescence. The zone of interest labeled 1 (Fig. 16A) corresponds with an emission peak at ~675 nm, though a visible chloroplast or any kind of structure in the brightfield image would be ideal to confirm the presence of chlorophyll. This is also complicated by the potential emission of Nile red in the same tissue.

Nile red is a well-established phenoxazine pigment that is typically used for protein gels or lipid staining in animal studies; it is known to work extremely well for staining lipid bodies in animal cells due to its low rate of precipitation and high specificity (Greenspan et al., 1985; Steinberg, 2009). However, as reported by Brundrett et al. (1991) and is clearly visible in Fig. 13E, Nile red stains phenolic compound-containing tissues (lignin) non-specifically, making it

somewhat more difficult to definitively identify lipid bodies in plants using this dye. Several large globular structures are visible in *C. gronovii* peduncle tissue, which are potentially large lipid bodies (Fig. 16). The two potential lipid bodies (regions of interest 2 and 3) have the same emission peak at ~665 nm. However, the expected emission peak for Nile red around 561 nm absorption is ~590 nm, below the range that was measured in these experiments (Greenspan et al., 1985). Thus, the emission visible in Fig. 16 is likely also chlorophyll, and a new experiment using the appropriate absorption/emission spectra would be necessary to get a better picture of lipid accumulation in this tissue.

Another subject of note that was unaddressed in this thesis and should be explored further is the possibility of gas exchange by *C. gronovii*. The abundance and structure of stomata in *C. gronovii* is not well documented, but this information would be valuable to understand whether *C. gronovii* is capable of capturing atmospheric CO_2. Anatomical studies could be supplemented by direct measures of CO_2 uptake in light, examining fruits as well as stems. Whole *C. gronovii* fruits appear to have very little ability to absorb CO_2 from the atmosphere (A. Cousins, personal communication, October 5, 2023), but individual seeds (separate from the fruit coat) may be able to do so. This would support the hypothesis by McNeal et al. (2007a,b) that RuBisCO is involved in recycling respiratory CO_2 that is already present within the plant.

Chapter 5

Conclusions

The ability to regulate nutrient allocation and storage is essential for all life, but especially so in sessile organisms like plants, which are entirely dependent on environmental conditions. This requires an incredible level of physiological flexibility to prevent the inefficient use of resources. This is perhaps even more important in parasitic plants, which are not only sessile but also dependent on the health and survival of a separate host plant. As such, it is clearly beneficial for parasitic plants—especially species growing in more disturbed, stochastic environments—to maintain many different modes of metabolism to guarantee survival. This thesis provides additional evidence that *C. gronovii*, typically considered holoparasitic, in fact maintains some aspects of photosynthesis that may be crucial to survival in disturbed areas. The ability to "hedge your bets" in this way, and supplement the nutrition received from a host with a limited degree of photosynthesis, is likely understudied in the field of parasitic plants, where parasites are often simply assigned "holoparasite" or "hemiparasite" designations. A better view of this distinction would be a spectrum of photosynthetic ability, with a plant's position determined by a variety of factors including gas exchange ability, chlorophyll content, gene losses, and the use of photosynthesis genes in canonical and non-canonical pathways, such as the RuBisCO shunt.

This last point is still unresolved in *C. gronovii*. The differential expression analyses conducted above are not enough to say that the pathway is definitively active or not, though the presence and activity of certain key genes (PRK, RBCS) is suggestive. Metabolomics studies

examining the accumulation of lipids and their $\delta^{13}C$ ratios would be necessary to understand whether seed lipids are significantly derived from RuBisCO activity.

This thesis also raises many interesting questions about the internal anatomy of *C. gronovii*, which is relatively understudied in the literature. In particular, the question of lipid accumulation in fruits remains open. Some studies such as Martinčová et al. (2019) have examined lipid localization in mature seeds, but the process of lipid and starch accumulation during fruit and seed development is still largely undescribed. Fluorescent dyes such as Nile red remain a powerful tool to visualize this, and anatomical studies using these dyes would be a very useful addition to potential metabolomics studies. However, use of these fluorescent dyes in *Cuscuta* would require some optimization (e.g., staining time, absorption/emission wavelengths, and knowledge of potential confounding factors such as nonspecific staining) due to their very infrequent use with this plant in the literature.

Finally, it is important to note that these results likely will not have an impact on the most prevalent (and extremely important) area of protecting crops from parasitic plants. Understanding the details of a parasite's metabolism is useful insofar as it reveals weaknesses that can be used to improve human livelihoods and food security. With a relatively benign parasite such as *C. gronovii*, the merit of this and future work is rather in a similar vein as that of conservation and natural history: understanding, categorizing, and ultimately protecting the incredible diversity of life on our planet.

Appendix A

Tissues of Interest

Table 7. QuantSeq libraries and corresponding tissues.

Library	Tissue description	Replicates
1.1	Dry seeds	4
1.2	Imbibed seeds, immediately after visible swelling	4
1.3	Imbibed seeds, 1 hour after swelling	3 (1 removed = 2)
2.1.1	Seedlings (24 hours after imbibing) – Shoot apex	4
2.1.2	Seedlings (24 hours after imbibing) – Radicular end	4
2.2.1	Starved seedling (5 days after imbibing) – Shoot apex	4 (1 removed = 3)
2.2.2	Starved seedling (5 days after imbibing) – Radicular end	4
3.1	Pre-haustoria – coiled stem (day 1)	4
3.2	Pre-haustoria – pre-haustoria (day 2)	4
4.1	Developing haustoria – removed from host (day 4)	4
4.2	Mature haustoria – removed from host (day 8)	4
5.1	Growing shoot tip, green	4
5.2	Stem base	4
5.3	Stem, adjacent to pre-haustoria (day 2)	4
5.4	Stem adjacent to developing (day 4) haustoria	4
5.5	Stem, adjacent to mature (day 8) haustoria	4
6.1	Pre-meiotic flower bud (calyx partially covering corolla)	4
6.2	Post-meiotic flower bud (calyx smaller than corolla)	4
6.3	Open flower	4
7.1	Green developing fruits, 7 days after flower opening	4
7.2	Brown mature fruits, more than 7 weeks after flower opening	4

Appendix B

Tool Settings and Sources for QuantSeq

Cutadapt settings (version 4.6)

```
cutadapt --json stats.json -a "QuantSeq FWD
adapter"="A{18}AGATCGGAAGAGCACACGTCTGAACTCCAGTCAC" -a "QuantSeq FWD adapter
w/out polyA"="AGATCGGAAGAGCACACGTCTGAACTCCAGTCAC" --output="outfile.fastq" --
error-rate=0.1 --times=1 --overlap=10 --action=trim --minimum-length=20 --
quality-cutoff=20 --poly-a "infile.fastq" > report.txt
```

RNA-STAR settings (version 2.7.11a)

```
STAR --genomeDir <genome_directory>
--readFilesIn <trimmed_reads.fastq> --outFilterType BySJout
--outFilterMultimapNmax 20 --alignSJoverhangMin 8
--alignSJDBoverhangMin 1 --outFilterMismatchNmax 999
--outFilterMismatchNoverLmax 0.6 --alignIntronMin 20
--alignIntronMax 1000000 --alignMatesGapMax 1000000
--outSAMattributes NH HI NM MD --outSAMtype BAM SortedByCoordinate
--outFileNamePrefix <outfile_prefix>
```

HTSeq-count settings (2.0.5)

```
htseq-count --mode=union --stranded=yes --minaqual=1 --type='gene' --
idattr='ID' --nonunique=none --order=name --secondary-alignments=ignore --
supplementary-alignments=ignore --counts_output=<output.tsv> --format=bam
<alignments.bam> <annotation.gff3>
```

A complete QuantSeq analysis workflow in Galaxy can be found below:

https://usegalaxy.eu/u/lgoubet-mccall/w/quantseq/json

Software sources

Anders, S., Pyl, P. T., & Huber, W. (2014). HTSeq—a python framework to work with high-throughput sequencing data. *Bioinformatics*, *31*(2), 166–169. https://doi.org/10.1093/bioinformatics/btu638

Dobin, A., Davis, C. A., Schlesinger, F., Drenkow, J., Zaleski, C., Jha, S., Batut, P., Chaisson, M., & Gingeras, T. R. (2012). Star: Ultrafast universal RNA-seq aligner. *Bioinformatics*, *29*(1), 15–21. https://doi.org/10.1093/bioinformatics/bts635

Love, M. I., Huber, W., & Anders, S. (2014). Moderated estimation of fold change and dispersion for RNA-seq data with deseq2. *Genome Biology*, *15*(12). https://doi.org/10.1186/s13059-014-0550-8

Martin, M. (2011). CUTADAPT removes adapter sequences from high-throughput sequencing reads. *EMBnet.Journal*, *17*(1), 10. https://doi.org/10.14806/ej.17.1.200

Okonechnikov, K., Conesa, A., & García-Alcalde, F. (2015). Qualimap 2: Advanced multi-sample quality control for high-throughput sequencing data. *Bioinformatics*, *32*(2), 292–294. https://doi.org/10.1093/bioinformatics/btv566

Posit Team. (2023). RStudio: Integrated Development Environment for R (Version 2023.12.1+402). Posit Software, PBC. Retrieved 2023, from http://www.posit.co/.

R Core Team. (2023). R: A Language and Environment for Statistical Computing (Version v4.3.0). R Foundation for Statistical Computing. Retrieved 2023, from https://www.r-project.org/.

The Galaxy Community (2022). The Galaxy Platform for Accessible, reproducible and collaborative biomedical analyses: 2022 update. *Nucleic Acids Research*, *50*(W1), W345–W351. https://doi.org/10.1093/nar/gkac247

Wickham, H. (2016). ggplot2: Elegant Graphics for Data Analysis. Springer-Verlag New York.

Appendix C

Annotation Evaluation Results

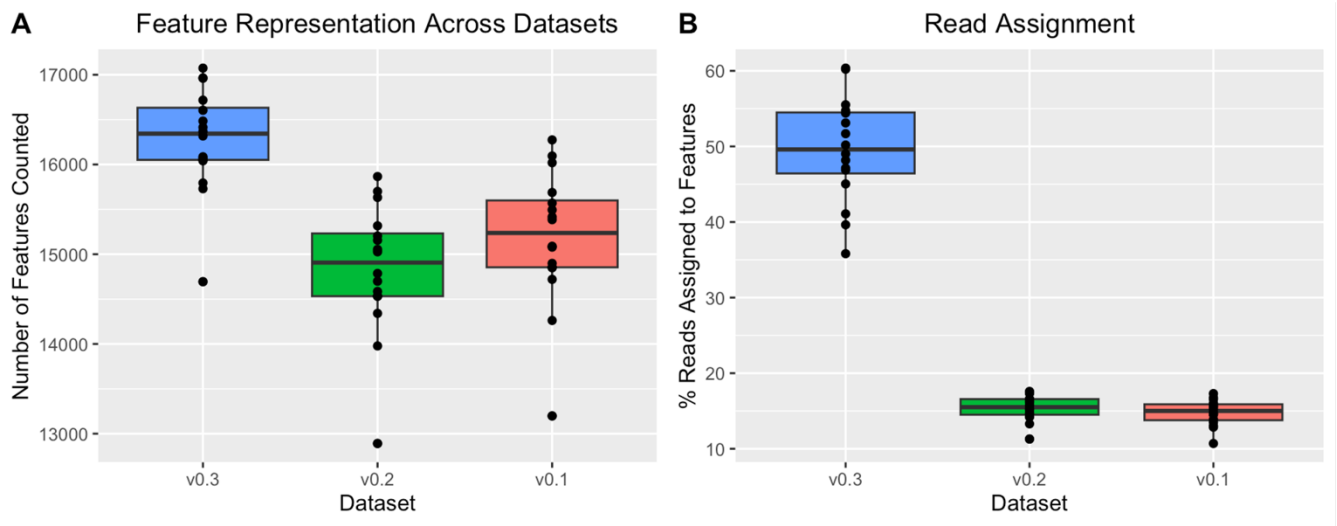

C

Dataset	# of total features	Average % of features with assigned reads
v0.3 PASA annotation	30291	53.72%
v0.2 TransDecoder annotation	33852	43.81%
v0.1 BRAKER annotation	30419	49.91%

D

Dataset	Average % reads assigned to features
v0.3 PASA annotation	49.56%
v0.2 TransDecoder annotation	15.41%
v0.1 BRAKER annotation	14.80%

Figure 18. Results of the evaluation for each version of the annotation, conducted with 16 of the 83 QuantSeq datasets (brown fruit, green fruit, stem base, and stem tip). The v0.3 version of the annotation, built by Juan Cerda using PASA, showed a significantly higher percentage of read assignment than the other versions, as well as a higher percentage of features with at least one read.

Appendix D

Genes of Interest

Table 8. Subset of *A. thaliana* genes of interest with homologs found in the JDC1 *C. gronovii* genome. Homologs were identified through CDS-versus-CDS reciprocal best hits using BLASTn.

TAIR Locus ID	Arabidopsis gene	Dataset
AT1G08940	AT1G08940	CBB cycle
AT1G56190	AT1G56190	CBB cycle
AT1G63290	AT1G63290	CBB cycle
AT2G25870	AT2G25870	CBB cycle
AT2G38740	AT2G38740	CBB cycle
AT2G45290	AT2G45290	CBB cycle
AT3G04880	DRT102	CBB cycle
AT2G21330	FBA1	CBB cycle
AT1G43670	FBP	CBB cycle
AT1G12900	GAPA-2	CBB cycle
AT1G13440	GAPC2	CBB cycle
AT2G01140	PDE345	CBB cycle
AT1G32060	PRK	CBB cycle
AT1G67090	RBCS1A	CBB cycle
AT5G61410	RPE	CBB cycle
AT1G71100	RSW10	CBB cycle
AT3G55800	SBPASE	CBB cycle
AT2G21170	TIM	CBB cycle
AT1G68220	AT1G68220	Chlorophyll synthesis
AT3G03890	AT3G03890	Chlorophyll synthesis
AT1G44446	CH1	Chlorophyll synthesis
AT4G18480	CHLI1	Chlorophyll synthesis
AT5G45930	CHLI2	Chlorophyll synthesis
AT4G25080	CHLM	Chlorophyll synthesis
AT5G26030	FC1	Chlorophyll synthesis
AT2G30390	FC2	Chlorophyll synthesis
AT3G51820	G4	Chlorophyll synthesis
AT3G59400	GUN4	Chlorophyll synthesis
AT5G13630	GUN5	Chlorophyll synthesis
AT2G26540	HEMD	Chlorophyll synthesis

AT3G14930	HEME1	Chlorophyll synthesis
AT2G40490	HEME2	Chlorophyll synthesis
AT4G03205	hemf2	Chlorophyll synthesis
AT1G69720	HO3	Chlorophyll synthesis
AT1G58300	HO4	Chlorophyll synthesis
AT3G09150	HY2	Chlorophyll synthesis
AT1G03475	LIN2	Chlorophyll synthesis
AT5G18660	PCB2	Chlorophyll synthesis
AT4G39920	POR	Chlorophyll synthesis
AT5G54190	PORA	Chlorophyll synthesis
AT4G27440	PORB	Chlorophyll synthesis
AT1G50170	SIRB	Chlorophyll synthesis
AT2G26670	TED4	Chlorophyll synthesis
AT1G66120	AAE11	FA synthesis
AT3G16170	AAE13	FA synthesis
AT3G16910	AAE7	FA synthesis
ArthCp031	accD	FA synthesis
AT1G62940	ACOS5	FA synthesis
AT3G05020	ACP1	FA synthesis
AT1G54580	ACP2	FA synthesis
AT1G54630	ACP3	FA synthesis
AT4G25050	ACP4	FA synthesis
AT5G27200	ACP5	FA synthesis
AT1G10310	AT1G10310	FA synthesis
AT1G24360	AT1G24360	FA synthesis
AT1G62610	AT1G62610	FA synthesis
AT1G63380	AT1G63380	FA synthesis
AT2G17845	AT2G17845	FA synthesis
AT2G22230	AT2G22230	FA synthesis
AT2G47245	AT2G47245	FA synthesis
AT3G02610	AT3G02610	FA synthesis
AT3G02620	AT3G02620	FA synthesis
AT3G02630	AT3G02630	FA synthesis
AT3G06460	AT3G06460	FA synthesis
AT3G55290	AT3G55290	FA synthesis
AT4G11030	AT4G11030	FA synthesis
AT5G10160	AT5G10160	FA synthesis
AT5G16230	AT5G16230	FA synthesis

AT5G16240	AT5G16240	FA synthesis
AT5G15530	BCCP2	FA synthesis
AT5G16390	CAC1	FA synthesis
AT5G35360	CAC2	FA synthesis
AT2G38040	CAC3	FA synthesis
AT2G30200	EMB3147	FA synthesis
AT1G43800	FTM1	FA synthesis
AT1G62640	KAS III	FA synthesis
AT5G46290	KASI	FA synthesis
AT2G47240	LACS1	FA synthesis
AT1G49430	LACS2	FA synthesis
AT1G64400	LACS3	FA synthesis
AT4G23850	LACS4	FA synthesis
AT3G05970	LACS6	FA synthesis
AT5G27600	LACS7	FA synthesis
AT2G04350	LACS8	FA synthesis
AT1G77590	LACS9	FA synthesis
AT2G05990	MOD1	FA synthesis
AT2G43710	SSI2	FA synthesis
AT4G04640	ATPC1	Photosynthesis
AT1G15700	ATPC2	Photosynthesis
AT4G09650	ATPD	Photosynthesis
AT1G29930	CAB1	Photosynthesis
AT1G29920	CAB2	Photosynthesis
AT1G20340	DRT112	Photosynthesis
AT3G54890	LHCA1	Photosynthesis
AT3G61470	LHCA2	Photosynthesis
AT1G61520	LHCA3	Photosynthesis
AT3G47470	LHCA4	Photosynthesis
AT1G45474	Lhca5	Photosynthesis
AT1G19150	Lhca6	Photosynthesis
AT2G05100	LHCB2.1	Photosynthesis
AT2G05070	LHCB2.2	Photosynthesis
AT3G27690	LHCB2.3	Photosynthesis
AT5G54270	LHCB3	Photosynthesis
AT5G01530	LHCB4.1	Photosynthesis
AT3G08940	LHCB4.2	Photosynthesis
AT2G40100	LHCB4.3	Photosynthesis

AT4G10340	LHCB5	Photosynthesis
AT1G15820	LHCB6	Photosynthesis
AT1G44575	NPQ4	Photosynthesis
AT4G03280	PETC	Photosynthesis
AT1G76100	PETE1	Photosynthesis
AT4G02770	PSAD-1	Photosynthesis
AT1G03130	PSAD-2	Photosynthesis
AT4G28750	PSAE-1	Photosynthesis
AT2G20260	PSAE-2	Photosynthesis
AT1G31330	PSAF	Photosynthesis
AT1G55670	PSAG	Photosynthesis
AT3G16140	PSAH-1	Photosynthesis
AT1G30380	PSAK	Photosynthesis
AT4G12800	PSAL	Photosynthesis
AT5G64040	PSAN	Photosynthesis
AT1G08380	PSAO	Photosynthesis
AT5G66570	PSBO1	Photosynthesis
AT3G50820	PSBO2	Photosynthesis
AT1G06680	PSBP-1	Photosynthesis
AT2G30790	PSBP-2	Photosynthesis
AT4G05180	PSBQ-2	Photosynthesis
AT1G79040	PSBR	Photosynthesis
AT2G30570	PSBW	Photosynthesis
AT2G06520	PSBX	Photosynthesis
AT1G67740	PSBY	Photosynthesis
AT1G12230	AT1G12230	RuBisCO shunt
AT2G36580	AT2G36580	RuBisCO shunt
AT3G01850	AT3G01850	RuBisCO shunt
AT3G04050	AT3G04050	RuBisCO shunt
AT3G25960	AT3G25960	RuBisCO shunt
AT3G30841	AT3G30841	RuBisCO shunt
AT3G52990	AT3G52990	RuBisCO shunt
AT3G55650	AT3G55650	RuBisCO shunt
AT3G55810	AT3G55810	RuBisCO shunt
AT3G60750	AT3G60750	RuBisCO shunt
AT4G09520	AT4G09520	RuBisCO shunt
AT4G26390	AT4G26390	RuBisCO shunt
AT5G08570	AT5G08570	RuBisCO shunt

AT5G56350	AT5G56350	RuBisCO shunt
AT5G63680	AT5G63680	RuBisCO shunt
AT3G04790	EMB3119	RuBisCO shunt
AT1G74030	ENO1	RuBisCO shunt
AT2G29560	ENOC	RuBisCO shunt
AT1G09780	iPGAM1	RuBisCO shunt
AT3G08590	iPGAM2	RuBisCO shunt
AT2G36530	LOS2	RuBisCO shunt
AT3G22960	PKP-ALPHA	RuBisCO shunt
AT5G52920	PKP-BETA1	RuBisCO shunt
AT1G32440	PKp3	RuBisCO shunt
AT2G01290	RPI2	RuBisCO shunt
AT5G13420	TRA2	RuBisCO shunt
AT1G63290	AT1G63290	RuBisCO shunt, CBB cycle
AT2G45290	AT2G45290	RuBisCO shunt, CBB cycle
AT3G04880	DRT102	RuBisCO shunt, CBB cycle
AT1G32060	PRK	RuBisCO shunt, CBB cycle
AT1G67090	RBCS1A	RuBisCO shunt, CBB cycle
AT5G38430	RBCS1B	RuBisCO shunt, CBB cycle
AT5G38420	RBCS2B	RuBisCO shunt, CBB cycle
AT5G38410	RBCS3B	RuBisCO shunt, CBB cycle
AT5G61410	RPE	RuBisCO shunt, CBB cycle
AT1G71100	RSW10	RuBisCO shunt, CBB cycle
AT1G35250	AT1G35250	TAG synthesis
AT1G35290	AT1G35290	TAG synthesis
AT1G68260	AT1G68260	TAG synthesis
AT1G68280	AT1G68280	TAG synthesis
AT3G02030	AT3G02030	TAG synthesis
AT3G11325	AT3G11325	TAG synthesis
AT3G26820	AT3G26820	TAG synthesis
AT3G44830	AT3G44830	TAG synthesis
AT3G49200	AT3G49200	TAG synthesis
AT3G49210	AT3G49210	TAG synthesis
AT4G24160	AT4G24160	TAG synthesis
AT5G12420	AT5G12420	TAG synthesis
AT5G41120	AT5G41120	TAG synthesis
AT5G41130	AT5G41130	TAG synthesis
AT4G30580	ATS2	TAG synthesis

AT3G51520	DGAT2	TAG synthesis
AT3G25110	FaTA	TAG synthesis
AT1G08510	FATB	TAG synthesis
AT1G06520	GPAT1	TAG synthesis
AT1G02390	GPAT2	TAG synthesis
AT4G01950	GPAT3	TAG synthesis
AT1G01610	GPAT4	TAG synthesis
AT3G11430	GPAT5	TAG synthesis
AT2G38110	GPAT6	TAG synthesis
AT5G06090	GPAT7	TAG synthesis
AT4G00400	GPAT8	TAG synthesis
AT5G60620	GPAT9	TAG synthesis
AT3G57650	LPAT2	TAG synthesis
AT1G51260	LPAT3	TAG synthesis
AT1G75020	LPAT4	TAG synthesis
AT3G18850	LPAT5	TAG synthesis
AT1G15080	LPP2	TAG synthesis
AT3G02600	LPP3	TAG synthesis
AT3G18220	LPP4	TAG synthesis
AT5G03080	LPPgamma	TAG synthesis
AT3G09560	PAH1	TAG synthesis
AT5G42870	PAH2	TAG synthesis
AT2G01180	PAP1	TAG synthesis
AT5G13640	PDAT	TAG synthesis
AT1G54570	PES1	TAG synthesis
AT3G26840	PES2	TAG synthesis
AT1G04010	PSAT1	TAG synthesis
AT3G58490	SPP1	TAG synthesis
AT2G19450	TAG1	TAG synthesis

Appendix E

Complete Gene Expression Results

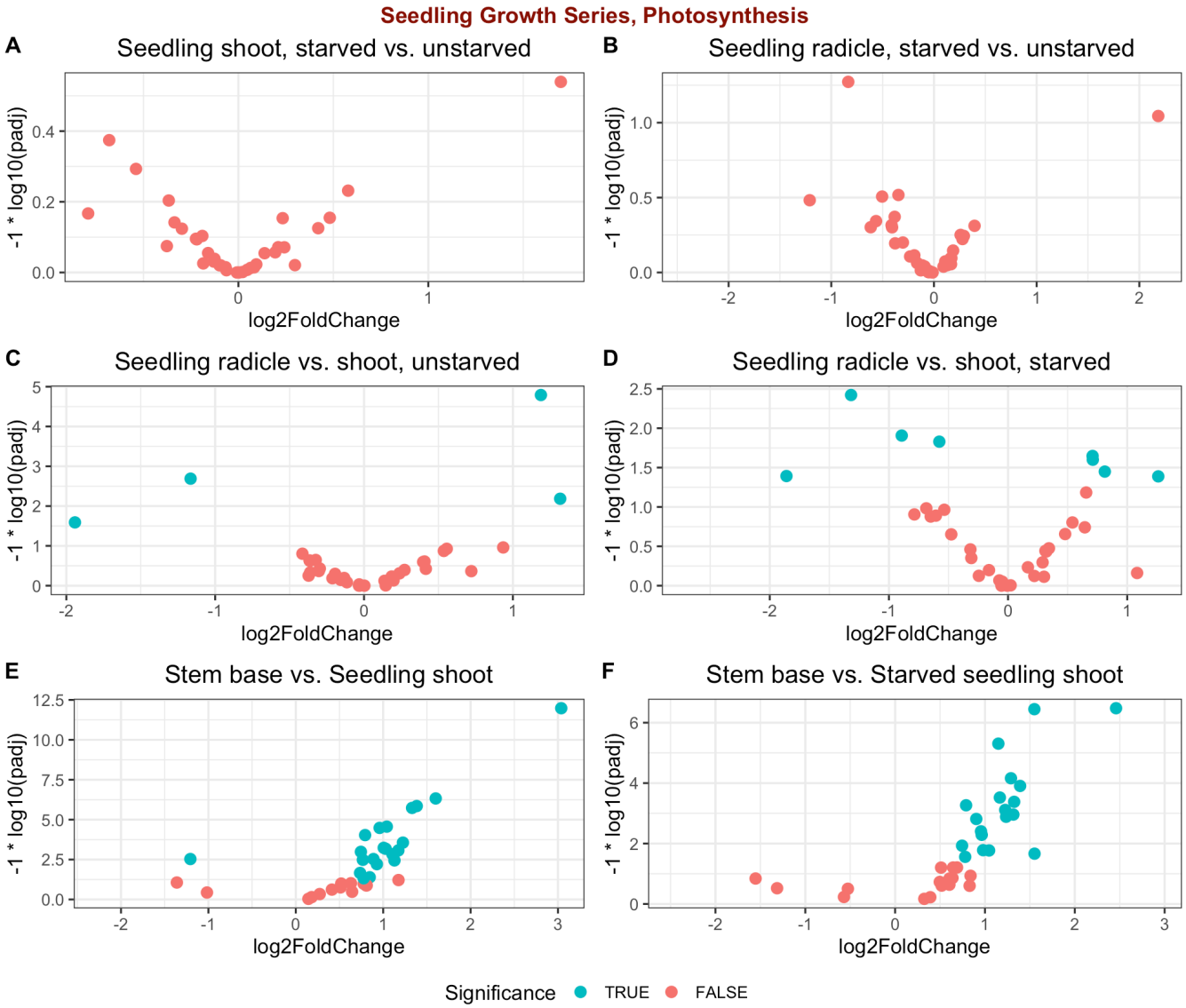

Figure 19. Expression of key photosynthesis genes across seedling tissues, shown with volcano plots. Various comparisons of the 4 relevant seedling tissues are shown (libraries 2.1.1, 2.1.2, 2.2.1, and 2.2.2).

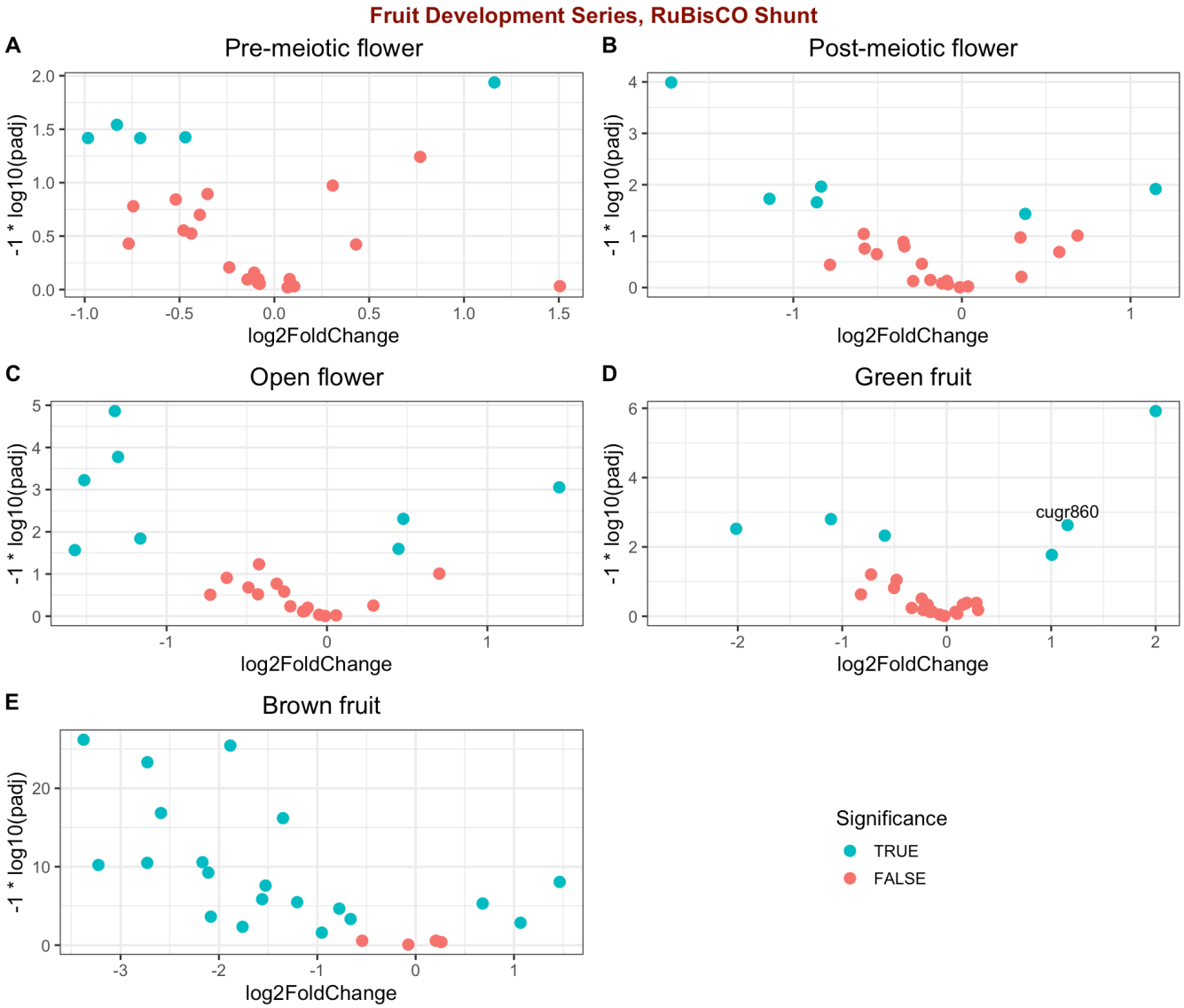

Figure 20. Expression of key RuBisCO shunt genes across fruit development, shown with volcano plots. All plots compare the expression of the tissue of interest against stem base. (D) cugr860 (homolog of RBCS) is labeled.

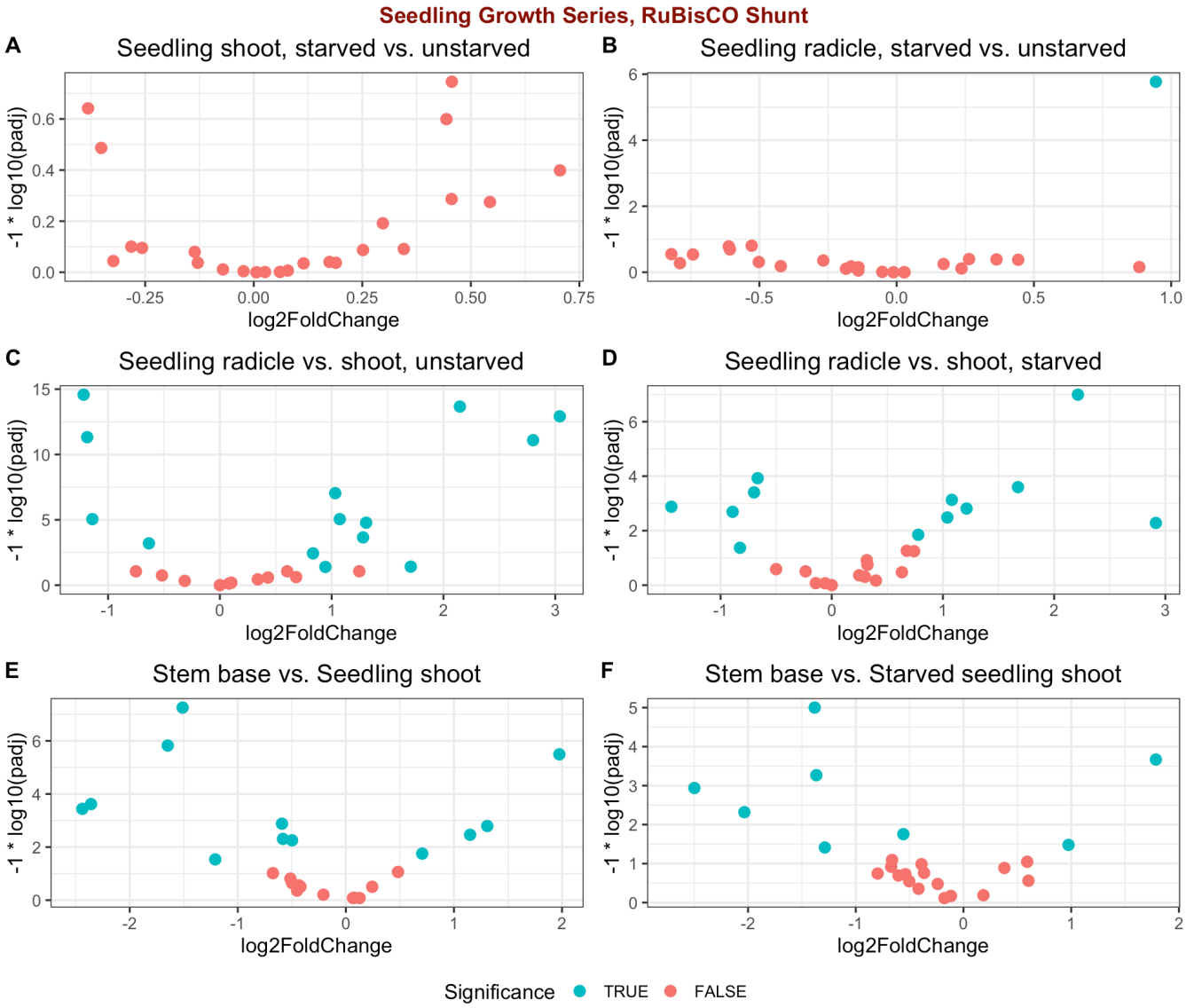

Figure 21. Expression of key RuBisCO shunt genes across seedling tissues.

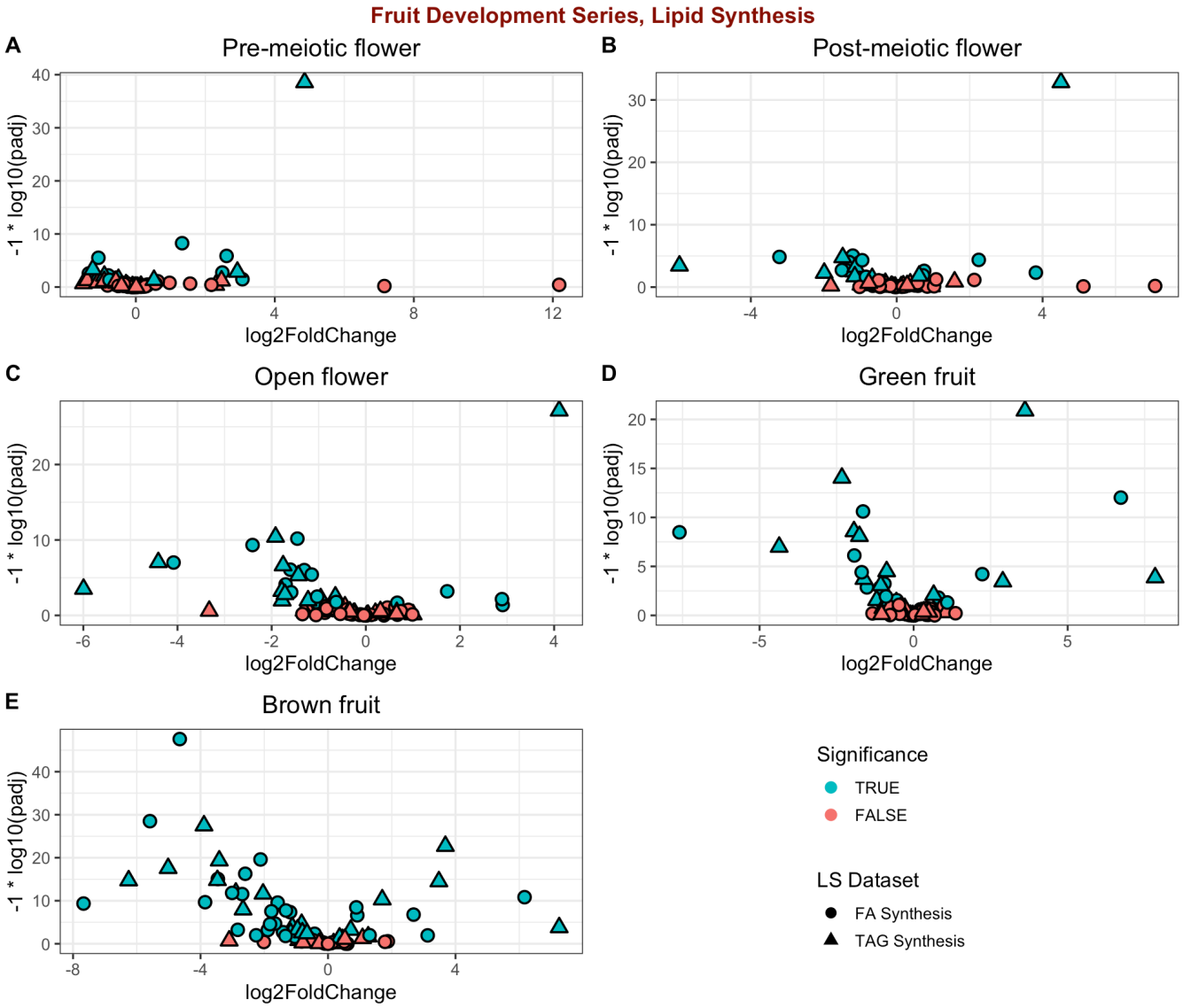

Figure 22. Expression of key lipid synthesis genes across fruit development.

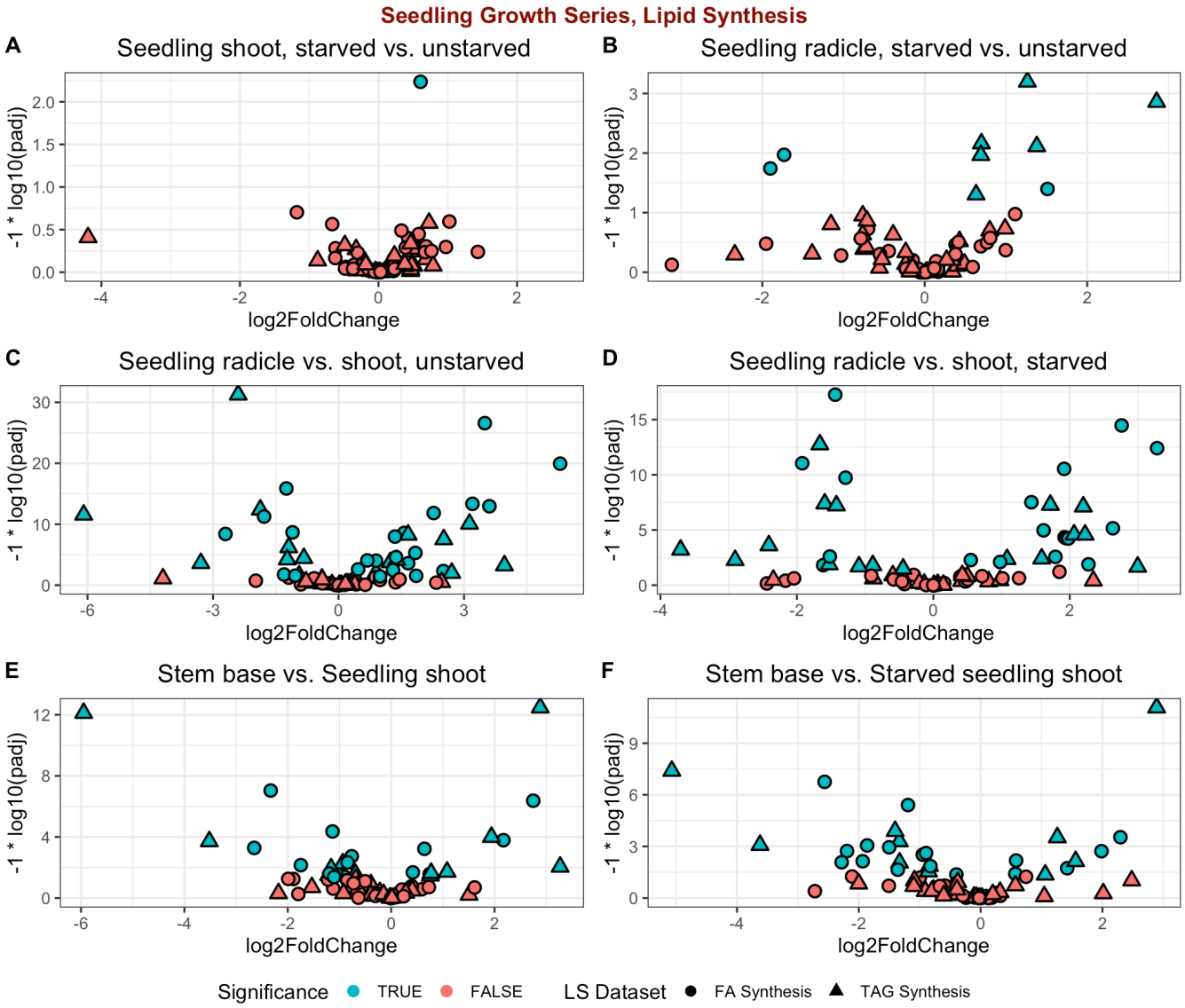

Figure 23. Expression of key lipid synthesis genes across seedling tissues.

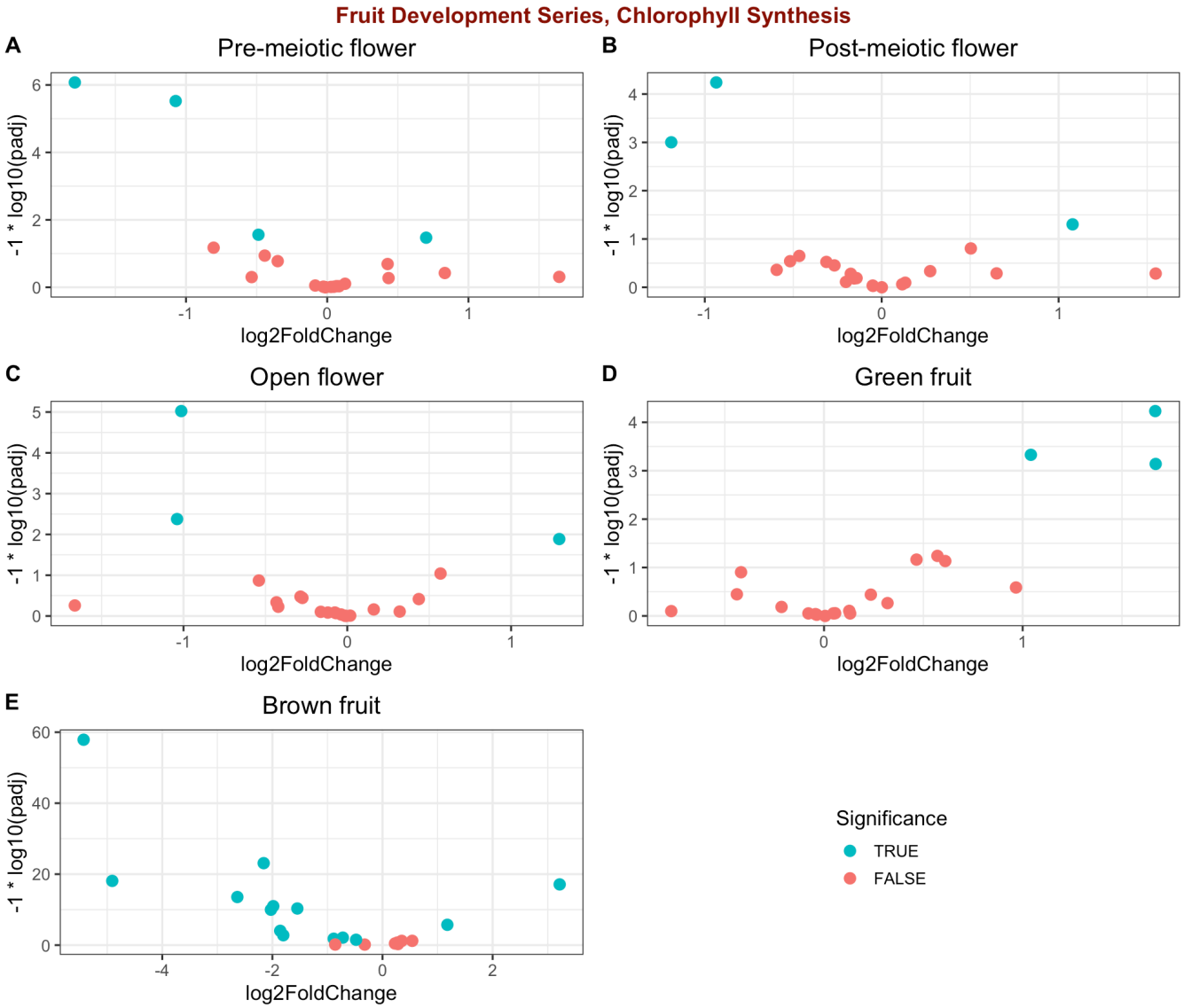

Figure 24. Expression of key chlorophyll synthesis genes across fruit development.

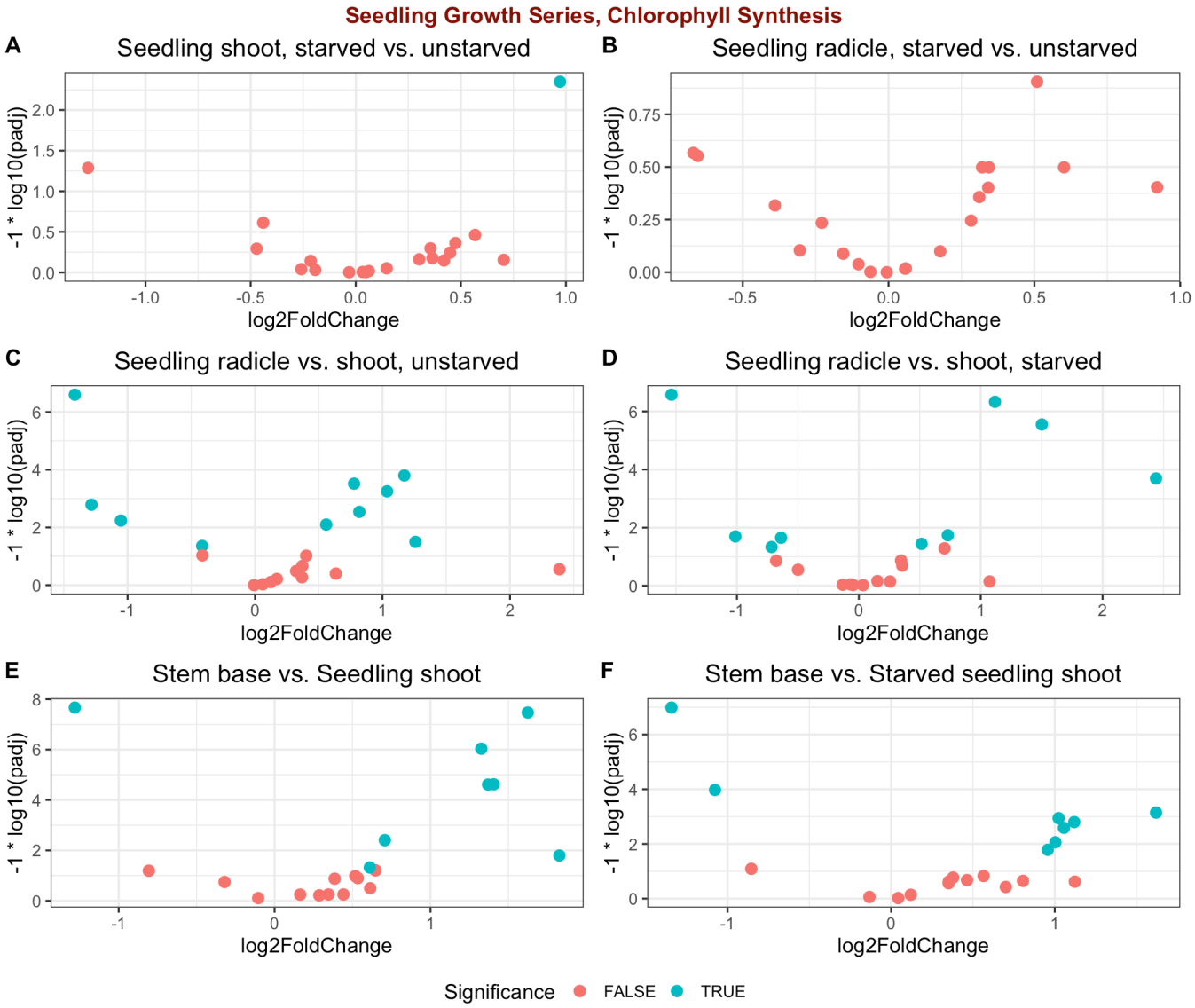

Figure 25. Expression of key chlorophyll synthesis genes across seedling tissues.

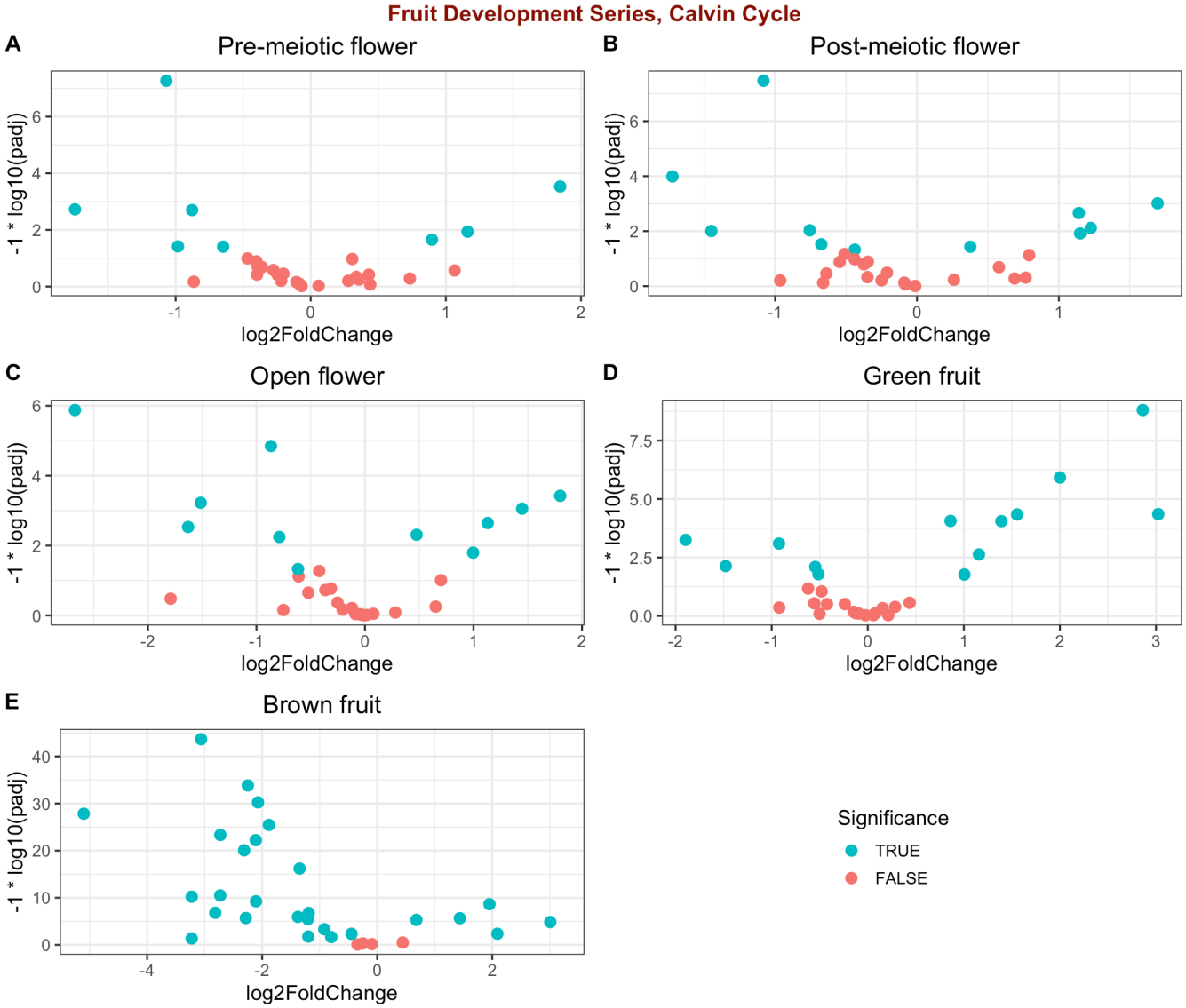

Figure 26. Expression of key Calvin cycle genes across fruit development.

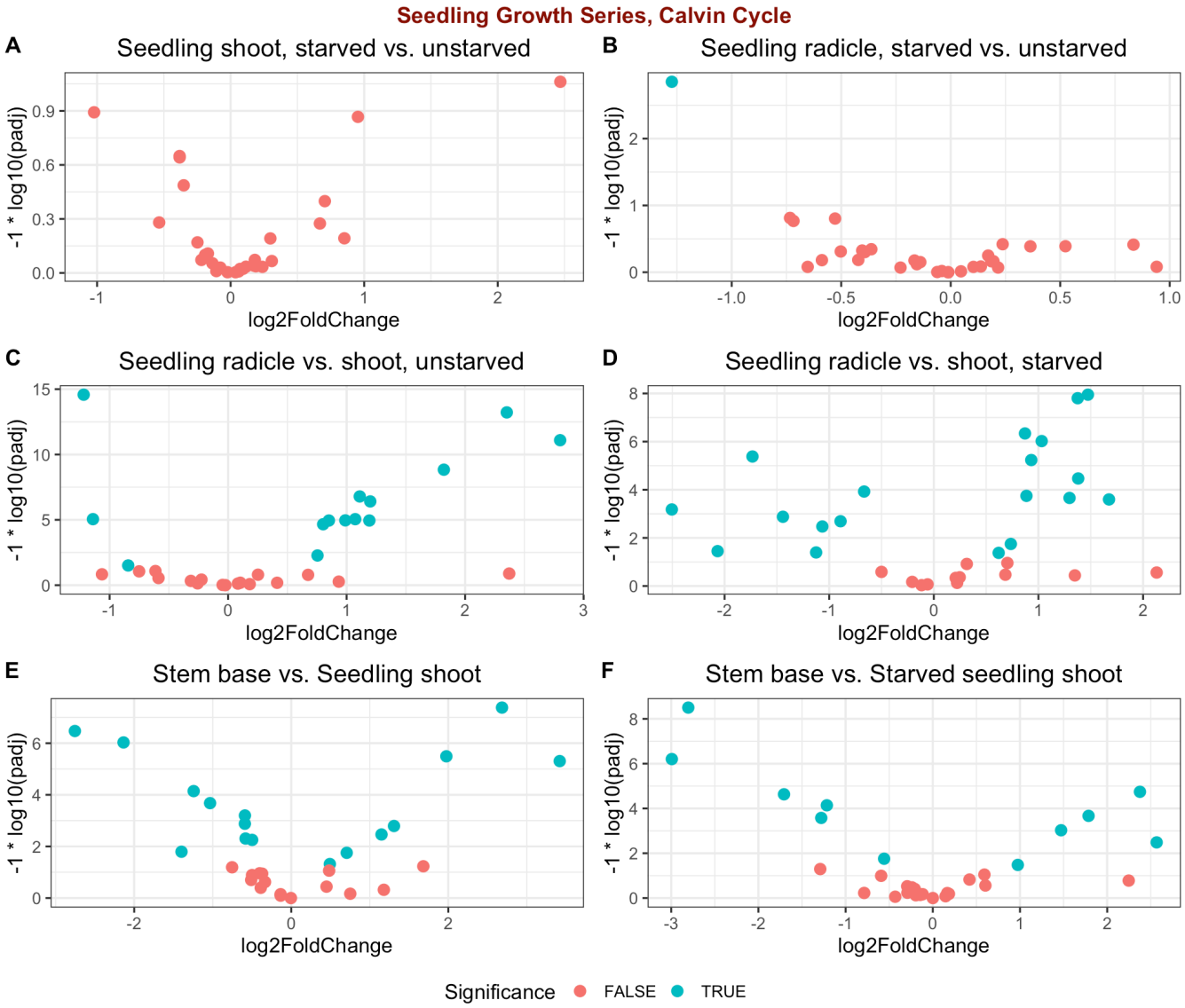

Figure 27. Expression of key Calvin cycle genes across seedling tissues.

BIBLIOGRAPHY

Arias-Agudelo, L. M., González, F., Isaza, J. P., Alzate, J. F., & Pabón-Mora, N. (2019). Plastome reduction and gene content in New World Pilostyles (Apodanthaceae) unveils high similarities to African and Australian congeners. *Molecular Phylogenetics and Evolution*, *135*, 193–202. https://doi.org/10.1016/j.ympev.2019.03.014

Barkman, T. J., McNeal, J. R., Lim, S. H., Coat, G., Croom, H. B., Young, N. D., & dePamphilis, C. W. (2007). Mitochondrial DNA suggests at least 11 origins of parasitism in angiosperms and reveals genomic chimerism in parasitic plants. *BMC Evolutionary Biology*, *7*(1). https://doi.org/10.1186/1471-2148-7-248

Baud, S. (2018). Seeds as oil factories. *Plant Reproduction*, *31*(3), 213–235. https://doi.org/10.1007/s00497-018-0325-6

Blankenship, R. E. (2010). Early Evolution of Photosynthesis. *Plant Physiology*, *154*(2), 434–438. https://doi.org/10.1104/pp.110.161687

Brundrett, M. C., Kendrick, B., & Peterson, C. A. (1991). Efficient Lipid Staining in Plant Material with Sudan Red 7B or Fluoral Yellow 088 in Polyethylene GlycolGlycerol. *Biotechnic and Histochemistry*, *66*(3), 111–116.

Cai, G., Kim, S. C., Li, J., Zhou, Y., & Wang, X. (2020). Transcriptional Regulation of Lipid Catabolism during Seedling Establishment. *Molecular Plant*, *13*(7), 984–1000. https://doi.org/10.1016/j.molp.2020.04.007

Cerda, J. D., & dePamphilis, C. W. (n.d.). *Unpublished*.

Chapman, K. D., & Ohlrogge, J. B. (2012). Compartmentation of triacylglycerol accumulation in plants. *Journal of Biological Chemistry*, *287*(4), 2288–2294. https://doi.org/10.1074/jbc.R111.290072

Costea, M., García, M. A., & Stefanović, S. (2015). A phylogenetically based infrageneric classification of the parasitic plant genus cuscuta (dodders, convolvulaceae). *Systematic Botany*, *40*(1), 269–285. https://doi.org/10.1600/036364415X686567

Costea, M., & Tardif, F. J. (2006). The biology of Canadian weeds. 133. Cuscuta campestris Yuncker, C. gronovii Willd. ex Schult., C. umbrosa Beyr. ex Hook., C. epithymum (L.) L. and C. epilinum Weihe. *Canadian Journal of Plant Science*, *81*(1), 293–316.

Costea, M., Wright, M. A. R., Glofcheskie, M., Genter, W., & Stefanović, S. (2023). Draining the Swamp Dodders: Systematics of Cuscuta gronovii s.l. (Subgenus Grammica, Sect. Oxycarpae). *Systematic Botany*, *48*(2), 325–345. https://doi.org/10.1600/036364423X16847773873206

Fernández-Aparicio, M., Delavault, P., & Timko, M. P. (2020). Management of infection by parasitic weeds: A review. *Plants*, *9*(9), 1–26. https://doi.org/10.3390/plants9091184

Furuhashi, T., Kojima, M., Sakakibara, H., Fukushima, A., Hirai, M. Y., & Furuhashi, K. (2014). Morphological and plant hormonal changes during parasitization by Cuscuta japonica on Momordica charantia. *Journal of Plant Interactions*, *9*(1), 220–232. https://doi.org/10.1080/17429145.2013.816790

Furuta, K. M., Xiang, L., Cui, S., & Yoshida, S. (2021). Molecular dissection of haustorium development in Orobanchaceae parasitic plants. *Plant Physiology*, *186*(3), 1424–1434. https://doi.org/10.1093/PLPHYS/KIAB153

Goyet, V., Wada, S., Cui, S., Wakatake, T., Shirasu, K., Montiel, G., Simier, P., & Yoshida, S. (2019). Haustorium Inducing Factors for Parasitic Orobanchaceae. *Frontiers in Plant Science*, *10*. https://doi.org/10.3389/fpls.2019.01056

Greenspan, P., Mayer, E. P., & Fowler, S. D. (1985). Nile Red: A Selective Fluorescent Stain for Intracellular Lipid Droplets. *The Journal of Cell Biology*, *100*, 965–973. http://rupress.org/jcb/article-pdf/100/3/965/1457917/965.pdf

Guo, X., Hu, X., Li, J., Shao, B., Wang, Y., Wang, L., Li, K., Lin, D., Wang, H., Gao, Z., Jiao, Y., Wen, Y., Ji, H., Ma, C., Ge, S., Jiang, W., & Jin, X. (2023). The Sapria himalayana genome provides new insights into the lifestyle of endoparasitic plants. *BMC Biology*, *21*(1). https://doi.org/10.1186/s12915-023-01620-3

Hawkins, C., Ginzburg, D., Zhao, K., Dwyer, W., Xue, B., Xu, A., Rice, S., Cole, B., Paley, S., Karp, P., & Rhee, S. Y. (2021). Plant Metabolic Network 15: A resource of genome-wide metabolism databases for 126 plants and algae. In *Journal of Integrative Plant Biology* (Vol. 63, Issue 11, pp. 1888–1905). John Wiley and Sons Inc. https://doi.org/10.1111/jipb.13163

Hegenauer, V., Fürst, U., Kaiser, B., Smoker, M., Zipfel, C., Felix, G., Stahl, M., & Albert, M. (2016). Detection of the plant parasite Cuscuta reflexa by a tomato cell surface receptor. *Science*, *353*(6298), 478–481.

Hölzl, G., & Dörmann, P. (2019). Chloroplast Lipids and their Biosynthesis. *Annual Review of Plant Biology*, *70*, 51–81. https://doi.org/10.1146/annurev-arplant-050718

Jąkalski, M., Minasiewicz, J., Caius, J., May, M., Selosse, M. A., & Delannoy, E. (2021). The Genomic Impact of Mycoheterotrophy in Orchids. *Frontiers in Plant Science*, *12*. https://doi.org/10.3389/fpls.2021.632033

Johnson, M. P. (2016). Photosynthesis. *Essays in Biochemistry*, *60*(3), 255–273. https://doi.org/10.1042/EBC20160016

Johnson, N. R., & Axtell, M. J. (2019). Small RNA warfare: exploring origins and function of trans-species microRNAs from the parasitic plant Cuscuta. *Current Opinion in Plant Biology*, *50*, 76–81. https://doi.org/10.1016/j.pbi.2019.03.014

Kazaz, S., Barthole, G., Domergue, F., Ettaki, H., To, A., Vasselon, D., de Vos, D., Belcram, K., Lepiniec, L., & Baud, S. (2020). Differential activation of partially redundant Δ9 stearoyl-ACP desaturase genes is critical for omega-9 monounsaturated fatty acid biosynthesis during seed development in arabidopsis. *Plant Cell*, *32*(11), 3613–3637. https://doi.org/10.1105/TPC.20.00554

Kelleway, J. J., Mazumder, D., Baldock, J. A., & Saintilan, N. (2018). Carbon isotope fractionation in the mangrove Avicennia marina has implications for food web and blue carbon research. *Estuarine, Coastal and Shelf Science*, *205*, 68–74. https://doi.org/10.1016/j.ecss.2018.03.011

Kristensen, D. M., Wolf, Y. I., Mushegian, A. R., & Koonin, E. V. (2011). Computational methods for Gene Orthology inference. *Briefings in Bioinformatics*, *12*(5), 379–391. https://doi.org/10.1093/bib/bbr030

Kubo, M., Udagawa, M., Nishikubo, N., Horiguchi, G., Yamaguchi, M., Ito, J., Mimura, T., Fukuda, H., & Demura, T. (2005). Transcription switches for protoxylem and metaxylem vessel formation. *Genes and Development*, *19*(16), 1855–1860. https://doi.org/10.1101/gad.1331305

Kuijt, J. (1969). Cuscuta, Cassytha, Lennoaceae, and Krameriaceae. In *The Biology of Parasitic Flowering Plants* (1st ed., pp. 136–157). University of California Press, Ltd.

Lanini, W. T., & Kogan, M. (2005). Biology and Management of Cuscuta in Crops. *Ciencia E Investigacion Agraria*, *32*(3), 127–141.

Lexogen GmbH. (2018). *QuantSeq 3' mRNA-Seq Integrated Data Analysis Pipelines on Bluebee® Genomics Platform User Guide*. www.lexogen.com

Lexogen GmbH. (2024). *Lexogen's Online FAQs*. Lexogen.

Li, N., Gügel, I. L., Giavalisco, P., Zeisler, V., Schreiber, L., Soll, J., & Philippar, K. (2015). FAX1, a Novel Membrane Protein Mediating Plastid Fatty Acid Export. *PLoS Biology*, *13*(2). https://doi.org/10.1371/journal.pbio.1002053

Li, Y., Xu, J., Li, G., Wan, S., Batistič, O., Sun, M., Zhang, Y., Scott, R., & Qi, B. (2019). Protein S-acyl transferase 15 is involved in seed triacylglycerol catabolism during early seedling growth in Arabidopsis. *Journal of Experimental Botany*, *70*(19), 5205–5216. https://doi.org/10.1093/jxb/erz282

Ludwig, M., Hartwell, J., Raines, C. A., & Simkin, A. J. (2024). The Calvin-Benson-Bassham cycle in C4 and Crassulacean acid metabolism species. *Seminars in Cell and Developmental Biology*, *155*, 10–22. https://doi.org/10.1016/j.semcdb.2023.07.013

Martinčová, M., Kaštier, P., Krasylenko, Y. A., Gajdoš, P., Čertík, M., Matušíková, I., & Blehová, A. (2019). Species-specific differences in architecture and chemical composition of dodder seeds. *Flora: Morphology, Distribution, Functional Ecology of Plants*, *256*, 61–68. https://doi.org/10.1016/j.flora.2019.04.010

McFadden, G. I. (2001). Primary and secondary endosymbiosis and the origin of plastids. *Journal of Phycology*, *37*(6), 951–959. https://doi.org/10.1046/j.1529-8817.2001.01126.x

McNeal, J. R., Arumugunathan, K., Kuehl, J. V., Boore, J. L., & dePamphilis, C. W. (2007a). Systematics and plastid genome evolution of the cryptically photosynthetic parasitic plant genus Cuscuta (Convolvulaceae). *BMC Biology*, *5*. https://doi.org/10.1186/1741-7007-5-55

McNeal, J. R., Kuehl, J. V., Boore, J. L., & De Pamphilis, C. W. (2007b). Complete plastid genome sequences suggest strong selection for retention of photosynthetic genes in the parasitic plant genus Cuscuta. *BMC Plant Biology*, *7*. https://doi.org/10.1186/1471-2229-7-57

Merckx, V., Bidartondo, M. I., & Hynson, N. A. (2009). Myco-heterotrophy: When fungi host plants. *Annals of Botany*, *104*(7), 1255–1261. https://doi.org/10.1093/aob/mcp235

Merckx, V., & Freudenstein, J. V. (2010). Evolution of Mycoheterotrophy in Plants: A Phylogenetic Perspective. *Source: The New Phytologist*, *185*(3), 605–609.

Molina, J., Hazzouri, K. M., Nickrent, D., Geisler, M., Meyer, R. S., Pentony, M. M., Flowers, J. M., Pelser, P., Barcelona, J., Inovejas, S. A., Uy, I., Yuan, W., Wilkins, O., Michel, C. I., Locklear, S., Concepcion, G. P., & Purugganan, M. D. (2014). Possible loss of the chloroplast genome in the parasitic flowering plant Rafflesia lagascae (Rafflesiaceae). *Molecular Biology and Evolution*, *31*(4), 793–803. https://doi.org/10.1093/molbev/msu051

Muñoz-Bertomeu, J., Cascales-Miñana, B., Mulet, J. M., Baroja-Fernández, E., Pozueta-Romero, J., Kuhn, J. M., Segura, J., & Ros, R. (2009). Plastidial glyceraldehyde-3-phosphate dehydrogenase deficiency leads to altered root development and affects the sugar and amino

acid balance in Arabidopsis. *Plant Physiology*, *151*(2), 541–558. https://doi.org/10.1104/pp.109.143701

Nickrent, D. L. (2020). Parasitic angiosperms: How often and how many? *Taxon*, *69*(1), 5–27. https://doi.org/10.1002/tax.12195

O'Leary, M. H. (1981). CARBON ISOTOPE FRACTIONATION IN PLANTS. *Phytochemistry*, *20*(4), 5–567.

Parry, M. A. J., Andralojc, P. J., Scales, J. C., Salvucci, M. E., Carmo-Silva, A. E., Alonso, H., & Whitney, S. M. (2013). Rubisco activity and regulation as targets for crop improvement. *Journal of Experimental Botany*, *64*(3), 717–730. https://doi.org/10.1093/jxb/err313

Plant Metabolic Network (PMN). (n.d.-a). Http://Www.Plantcyc.Org/. Retrieved March 9, 2024, from https://pmn.plantcyc.org/ARA/NEW-IMAGE?object=PWY-5723&redirect=T

Plant Metabolic Network (PMN). (n.d.-b). Http://Www.Plantcyc.Org/. Retrieved March 9, 2024, from https://pmn.plantcyc.org/PLANT/NEW-IMAGE?type=PATHWAY&object=CALVIN-PWY

Press, M. C., & Phoenix, G. K. (2005). Impacts of parasitic plants on natural communities. *New Phytologist*, *166*(3), 737–751. https://doi.org/10.1111/j.1469-8137.2005.01358.x

Sánchez-Baracaldo, P., Raven, J. A., Pisani, D., & Knoll, A. H. (2017). Early photosynthetic eukaryotes inhabited low-salinity habitats. *PNAS*, *114*(37), E7737–E7745. https://doi.org/10.5061/dryad.421p2

Sandler, H. A. (2010). Managing Cuscuta gronovii (swamp dodder) in cranberry requires an integrated approach. *Sustainability*, *2*(2), 660–683. https://doi.org/10.3390/su2020660

Santos, E. A. V., Nurit-Silva, K., Arruda, E. C. P., & Leite, A. V. (2023). Morphoanatomical and histochemical study of Ipomoea hederifolia L. (Convolvulaceae). *Anales de Biología*, *45*, 9–21. https://doi.org/10.6018/analesbio.45.02

Sato, S., Nakamura, Y., Kaneko, T., Asamizu, E., & Tabata, S. (1999). Complete Structure of the Chloroplast Genome of Arabidopsis thaliana. *DNA RESEARCH*, *6*, 283–290. http://www.kazusa.or.jp/arabi/.

Schmidt, O., & Scrimgeour, C. M. (2001). A simple urea leaf-feeding method for the production of ^{13}C and ^{15}N labelled plant material. *Plant and Soil*, *229*(2), 197–202. https://about.jstor.org/terms

Schwender, J., Goffman, F., Ohlrogge, J. B., & Shachar-Hill, Y. (2004). Rubisco without the Calvin cycle improves the carbon efficiency of developing green seeds. *Nature*, *432*(7018), 779–782. https://doi.org/doi:10.1038/nature03145

Shahid, S., Kim, G., Johnson, N. R., Wafula, E., Wang, F., Coruh, C., Bernal-Galeano, V., Phifer, T., dePamphilis, C. W., Westwood, J. H., & Axtell, M. J. (2018). MicroRNAs from the parasitic plant Cuscuta campestris target host messenger RNAs. *Nature*, *553*(7686), 82–85. https://doi.org/10.1038/nature25027

Shen, G., Liu, N., Zhang, J., Xu, Y., Baldwin, I. T., & Wu, J. (2009). Cuscuta australis (dodder) parasite eavesdrops on the host plants' FT signals to flower. *PNAS*, *117*. https://doi.org/10.1073/pnas.2009445117/-/DCSupplemental

Simkin, A. J., Alqurashi, M., Lopez-Calcagno, P. E., Headland, L. R., & Raines, C. A. (2023). Glyceraldehyde-3-phosphate dehydrogenase subunits A and B are essential to maintain

photosynthetic efficiency. *Plant Physiology*, *192*(4), 2989–3000. https://doi.org/10.1093/plphys/kiad256

Simões, A. R. G., Eserman, L. A., Zuntini, A. R., Chatrou, L. W., Utteridge, T. M. A., Maurin, O., Rokni, S., Roy, S., Forest, F., Baker, W. J., & Stefanović, S. (2022). A Bird's Eye View of the Systematics of Convolvulaceae: Novel Insights From Nuclear Genomic Data. *Frontiers in Plant Science*, *13*. https://doi.org/10.3389/fpls.2022.889988

Stefanović, S., Kuzmina, M., & Costea, M. (2007). Delimitation of major lineages within Cuscuta subgenus Grammica (Convolvulaceae) using plastid and nuclear DNA sequences. *American Journal of Botany*, *94*(4), 568–589. https://doi.org/10.3732/ajb.94.4.568

Steinberg, T. H. (2009). Protein Gel Staining Methods. An Introduction and Overview. In *Methods in Enzymology* (Vol. 463, Issue C, pp. 541–563). Academic Press Inc. https://doi.org/10.1016/S0076-6879(09)63031-7

Taniguchi, M., & Lindsey, J. S. (2021). Absorption and Fluorescence Spectral Database of Chlorophylls and Analogues. *Photochemistry and Photobiology*, *97*(1), 136–165. https://doi.org/10.1111/php.13319

Teixeira-Costa, L., Davis, C. C., & Ceccantini, G. (2021). Striking developmental convergence in angiosperm endoparasites. *American Journal of Botany*, *108*(5), 756–768. https://doi.org/10.1002/ajb2.1658

Timilsena, P. R., Barrett, C. F., Piñeyro-Nelson, A., Wafula, E. K., Ayyampalayam, S., McNeal, J. R., Yukawa, T., Givnish, T. J., Graham, S. W., Pires, J. C., Davis, J. I., Ané, C., Stevenson, D. W., Leebens-Mack, J., Martínez-Salas, E., Álvarez-Buylla, E. R., & dePamphilis, C. W. (2023). Phylotranscriptomic Analyses of Mycoheterotrophic Monocots Show a Continuum

of Convergent Evolutionary Changes in Expressed Nuclear Genes From Three Independent Nonphotosynthetic Lineages. *Genome Biology and Evolution*, *15*(1). https://doi.org/10.1093/gbe/evac183

Tyagi, A. K., & Gaur, T. (2003). Light Regulation of Nuclear Photosynthetic Genes in Higher Plants. *Critical Reviews in Plant Sciences*, *22*(5), 417–452. https://doi.org/10.1080/07352680390243503

Vogel, A., Schwacke, R., Denton, A. K., Usadel, B., Hollmann, J., Fischer, K., Bolger, A., Schmidt, M. H. W., Bolger, M. E., Gundlach, H., Mayer, K. F. X., Weiss-Schneeweiss, H., Temsch, E. M., & Krause, K. (2018). Footprints of parasitism in the genome of the parasitic flowering plant Cuscuta campestris. *Nature Communications*, *9*(1). https://doi.org/10.1038/s41467-018-04344-z

Waese, J., Fan, J., Pasha, A., Yu, H., Fucile, G., Shi, R., Cumming, M., Kelley, L. A., Sternberg, M. J., Krishnakumar, V., Ferlanti, E., Miller, J., Town, C., Stuerzlinger, W., & Provart, N. J. (2017). ePlant: Visualizing and exploring multiple levels of data for hypothesis generation in plant biology. *Plant Cell*, *29*(8), 1806–1821. https://doi.org/10.1105/tpc.17.00073

Wicke, S., & Naumann, J. (2018). Molecular Evolution of Plastid Genomes in Parasitic Flowering Plants. In *Advances in Botanical Research* (Vol. 85, pp. 315–347). Academic Press Inc. https://doi.org/10.1016/bs.abr.2017.11.014

Wicke, S., Schneeweiss, G. M., dePamphilis, C. W., Müller, K. F., & Quandt, D. (2011). The evolution of the plastid chromosome in land plants: Gene content, gene order, gene function. *Plant Molecular Biology*, *76*(3–5), 273–297. https://doi.org/10.1007/s11103-011-9762-4

Yuncker, T. G. (1932). The Genus Cuscuta. *Memoirs of the Torrey Botanical Club*, *18*(2), 113–331.

Zhang, H., Florentine, S., & Tennakoon, K. U. (2022). The Angiosperm Stem Hemiparasitic Genus Cassytha (Lauraceae) and Its Host Interactions: A Review. *Frontiers in Plant Science*, *13*. https://doi.org/10.3389/fpls.2022.864110